Accepted Manuscript

http://dx.doi.org/10.1039/B909870D

Weber, J.; Schmedt auf der Günne, J. Calculation of NMR parameters in ionic solids by an improved selfconsistent embedded cluster method. *Phys. Chem. Chem. Phys.* **2010**, *12*, 583–603.

– Reproduced by permission of the PCCP Owner Societies

Graphical Abstract

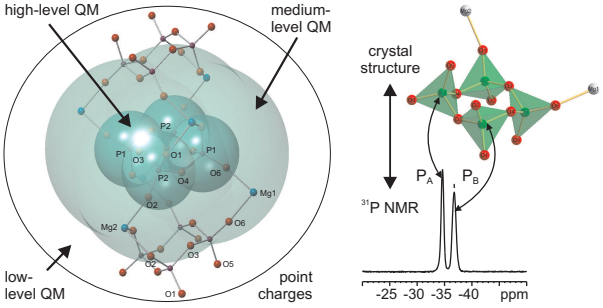

Calculation of NMR properties in solids by a self-consistent embedded cluster scheme that avoids empirical parameters and uses a semi-automatized cluster setup with locally dense basis.

Calculation of NMR parameters in ionic solids by an improved self-consistent embedded cluster method

Johannes Weber and
Jörn Schmedt auf der Günne†
Department of Chemistry and Biochemistry, Ludwig-Maximilians-Universität, D-81377 Munich, Germany.

Abstract

An new embedded cluster method (*extended embedded ion method*=EEIM) for the calculation of NMR properties in non-conducting crystals is presented. It is similar to the Embedded Ion Method (EIM)[1] in the way of embedding the quantum chemically treated part in an exact, self-consistent Madelung potential, but requires no empirical parameters. The method is put in relation to already existing cluster models which are classified in a brief review. The influence of the cluster boundary and the cluster charge is investigated, which leads to a better understanding of deficiencies in EIM. A recipe for an improved semi-automated cluster setup is proposed which allows the treatment of crystals composed of highly charged ions and covalent networks. EIM and EEIM results for ^{19}F and ^{31}P shielding tensors in NaF and in four different magnesium phosphates are compared with experimental values from solid state MAS NMR, some of which are measured here for the first time. The quantum part of the clusters is treated at hybride DFT level (mPW1PW) with atomic basis sets up to 6-311G(3df,3pd). The improved agreement of EEIM allows new signal assignments for the different P-sites in $Mg_2P_4O_{12}$, α-$Mg_2P_2O_7$ and MgP_4O_{11}. Conversion equations of the type $\sigma = A+B\cdot\delta$ between calculated absolute magnetic shieldings σ and the corresponding experimental chemical shifts δ are obtained independently from linear regressions of plots of isotropically averaged σ versus δ values on 19 ^{31}P signals of small molecules.

Keywords: solid state magic angle spinning NMR, magnesium phosphates, quantum chemical calculations, hybride density functional theory, self-consistent cluster embedding scheme, point charges, lattice potential, Madelung potential, chemical shift anisotropy

† author to whom correspondence should be addressed, email: gunnej@cup.uni-muenchen.de

1 Introduction

Nuclear magnetic resonance (NMR) spectroscopy is one of the most powerful experimental techniques for the elucidation of the structure of chemical compounds in various states of aggregation. In recent years, extensive progress has been achieved especially in the field of solid state NMR spectroscopy. In principle, information about connectivities, atomic distances[2], bond angles[3] and dihedral angles[4] can be extracted from solid state NMR data, which motivated the idea of a NMR crystallography[5]. But rather than thinking of a replacement for established X-ray diffraction techniques NMR should be regarded as a complementary tool which possesses the outstanding feature that it probes the sample locally with unequaled resolution power. This makes the method applicable to disordered and amorphous solids, too. While it is known that tiny changes in the local environment of an observed nucleus cause significant shifts of its resonance frequency, its prediction and understanding are often not straight forward. For this reason empirical correlations deduced from tables of assigned experimental spectra are very important[6,7]. In many cases no comparable data are available or it seems that simple relations do not exist[8]. An extremely useful tool to fill this gap consists in accurate quantum chemical calculations of NMR properties from first principles, which give an immediate relationship to the structure without the necessity of relying on empirical parameters. This allows the assignment of NMR signals to atomic sites in uncommon or difficult cases, leads to a deeper insight of empirical correlations and allows to predict spectra for different structural models.

While semiquantitative calculations of NMR properties are fairly routine for ordinary small molecules in the gas phase nowadays[9], the situation is not so favorable for ionic solids where far distant Coulomb interactions are present and the number of independent particles, i.e. the system size, is usually much bigger. The effect of Coulomb interactions on NMR shielding tensors $\overleftrightarrow{\sigma}$ can be sizeable, especially for highly polarizable systems. Two basic routes have been proposed for the calculation of $\overleftrightarrow{\sigma}$ in crystalline solids. The first takes full account of the translational crystal symmetry at quantum mechanical level and uses *periodic boundary conditions* to obtain the electronic wave function[10]. The second is based on a *cluster modelling ansatz*[1].

In the last few years periodic boundary calculations have become popular in the solid state NMR community, because two quantum chemical codes have been made available to the public, namely the CPMD program[11] with the NMR specific extensions by Sebastiani, Parinello and others[12] and the CASTEP or PARATEC program[13,14] with the GIPAW extension by Mauri, Pickard and others[10,15]. Impressive correlations between experimental and simulated shielding tensor components have shown that the predictive power of theoretical calculations has reached the precision necessary for practical applications. Still some problems remain which, we believe, are inherent to the underlying approximations and methodology. In general, periodic boundary calculations are expensive for big unit cells, because the entire cell is treated quantum mechanically. In a recent paper the current limit for GIPAW is specified to around 900 electrons per unit cell[16], which is reached quickly for larger cells con-

taining heavy atoms. A second issue is the description of the atomic core region by pseudo-potentials. Since the biggest contribution to the NMR shielding tensor comes from electrons close to the observed nucleus, any approximation to the core region is a delicate issue[17,18]. The GIPAW approach solves the core problem to some extend by restoring an all-electron description in the core region but comes at additional expense. Under this perspective calculations following the *cluster modelling ansatz* are an interesting alternative, because they can exploit the local nature of NMR properties.

The aim of this article is to show how increased benefit can be taken from the cluster approach in NMR shielding tensor calculations on crystalline solids. To this end we review advantages and disadvantages of different cluster implementations in section 2. In section 3 we present a new cluster model, which is based on the Embedded Ion Method (EIM) by Stueber, Grant and others[1,19,20]. The EIM is one of the more advanced cluster models available at the time and – in contrast to what its name might suggest – also applicable to uncharged quantum clusters[21]. Taking the simple system sodium fluoride (NaF) as an example we demonstrate that conceptual difficulties of EIM appear in the choice of charges attributed to the quantum cluster as well as to point charges building up the embedding electrostatic field. Moreover, the influence of the cluster boundary is investigated. This leads to the derivation of detailed prescriptions for the construction of improved clusters. Together with the realization of a semi-automated cluster construction procedure this gives rise to what we call the Extended Embedded Ion Method (EEIM). Finally, we validate the EEIM and the EIM against a set of experimental ^{31}P chemical shift tensor components of magnesium phosphates ($Mg_2P_4O_{12}$, Mg_3PO_4, α-$Mg_2P_2O_7$, and MgP_4O_{11}) in section 6.

2 Overview of existing cluster models

A review of cluster modelling schemes has been published recently[22]. Most of the works cited therein are focussed on the optimization of structures. Cluster calculations with focus on NMR properties have been reviewed in[1]. Unmentioned in either review are the references[7,23–31] that we found to be important in connection with our work. Here, we want to work out a systematic classification of different schemes with emphasis on NMR.

The basic idea of cluster modelling is to cut the relevant region (the *cluster*) containing the nuclei of interest out of the solid and to perform a non-periodic, molecular calculation on it. The main advantages of cluster calculations over periodic calculations are

A1. their low computational cost. A cluster *ansatz* benefits from the fact that NMR properties are rather local quantities, which leads to linear scaling behavior with respect to the unit cell size.

A2. the general availability of a larger number of non-periodic quantum chemical programs capable of doing NMR calculations, e.g.[32–38]. (In contrast there are

only the few periodic programs mentioned in the introduction.)

and apart from these economical aspects

A3. a larger variety of quantum chemical models. For example explicitly correlated *ab initio* methods necessary for systems with static electron correlation[9,39] or explicitly relativistic methods for systems with heavy nuclei are available[40].

A4. a larger variety of implemented properties, as for example the calculation of indirect nuclear spin-spin couplings at different levels of sophistication which is available in several packages.[33–36,41,42]. †

A5. the easily achievable modelling of non-ideal crystals with defects or impurities

The disadvantages of cluster calculations are

D1. the neglect of the translational symmetry of the wave function and often also the loss of local (point group) symmetry of the nuclei under investigation

D2. the approximate treatment or even full neglect of long range interactions

D3. the lack of proper boundary conditions/constraints as e.g. the correct charge of the system

D4. the large number of parameters that needs to be set, such as the cluster size (vs expense), the cluster charge, the choice of atomic basis functions, the quantum chemical model and the way of cluster embedding.

Despite of the basic deficiencies the results obtained from cluster calculations can be surprisingly good, because NMR properties are local quantities in the sense that the main contributions are determined by the electronic wave function in a restricted region around the nuclei of interest. This has been recognized already in early calculations of NMR parameters[44–48] and was verified later for a number of model systems[49–52]. Further theoretical foundation of the local approximation is given in section 1 of the supplemental material.

The quality of the results depends critically on the cluster setup. In the following we propose a classification scheme for the many types of cluster calculations that have been presented in the past. It may be used as a rough estimate for the quality of a cluster calculation. A graphical overview is given in Fig. 1.

† In fact this property has been recently incorporated in a periodic code using a super-cell technique[43]. The reported computational resources for extended systems are quite considerable, however.

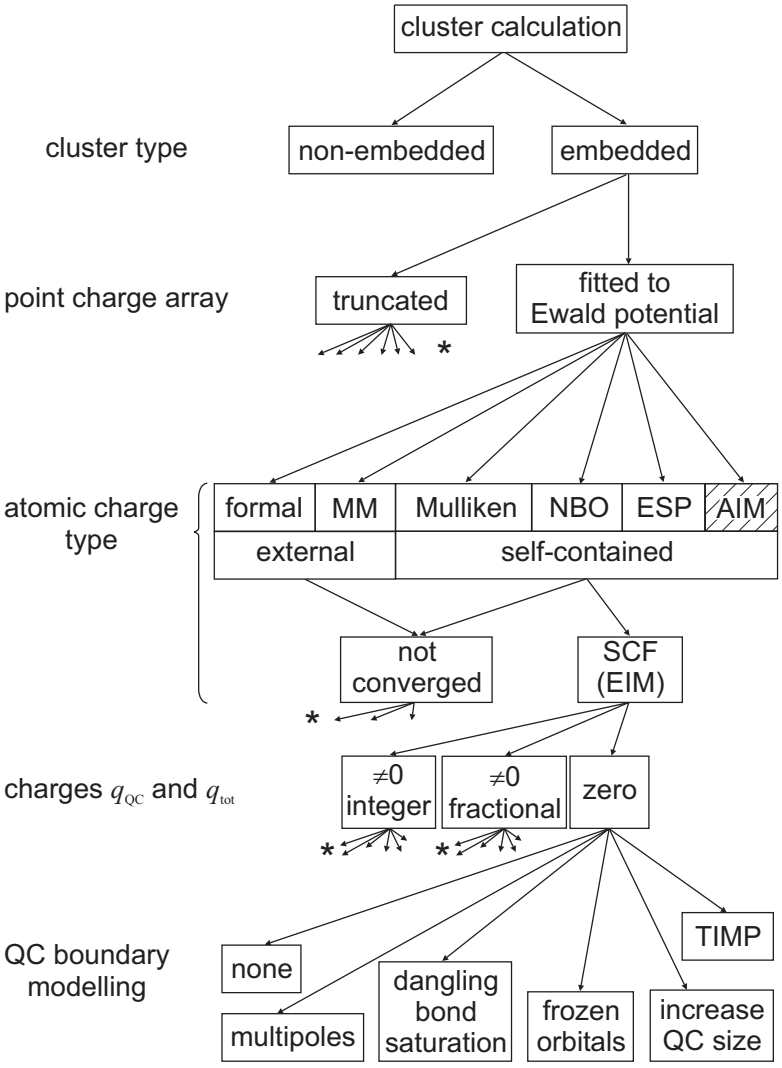

Figure 1: Tree diagram for types of cluster calculations. Acronyms and variables are explained in the text. Unconnected arrows marked by a star (*) indicate that the branch continues in the same way as the neighboring branch.

Two prototypes of cluster calculations can be distinguished: The first type are *non-embedded cluster calculations*, where all atoms inside the cluster are treated quantum mechanically (at the same level) and all remaining atoms of the solid are ignored, see e.g.[7]. Obviously, long range interactions are disregarded in this approximation. While this might be acceptable for magnetic shielding calculations on non-polar molecular crystals, it is not sufficient for ionic systems, where long range coulomb interactions have proven to be important[30,46,53]. In such cases the achievable size of the quantum cluster (QC) is usually too small to arrive at converged results.

The second type are *embedded cluster calculations*. Here, long range interactions are approximated electrostatically by embedding the QC in an array of point charges

$\{q_j(\mathbf{r}_j)\}$, $j = 1, 2, \ldots M$, which mimic the effect of atoms outside the QC by adding a potential

$$V(\mathbf{r}_i) = \sum_{j \notin QC}^{M} \frac{q_j}{r_{ij}} \quad \text{with } r_{ij} = |\mathbf{r}_i - \mathbf{r}_j| \tag{1}$$

at a point $\mathbf{r}_i$ in the quantum region. Several recipes have been given for the determination of the number M of point charges, their magnitude q_j, and their location $\mathbf{r}_j$ [19,24,29,54–56]. The q_j are not necessarily identical to atomic charges and the locations $\mathbf{r}_j$ do not necessarily coincide with nuclear positions[54]. On the one hand, the identification as a classical substitute for an atomic site in a crystal is appealing, because each point charge has a concrete meaning then. On the other hand, an infinite number of point charges would have to be generated around the QC and summed according to (1) in order to represent an ideal crystal, which is impossible in practice.

At this point the embedded cluster calculations split in further subclasses: Some schemes simply truncate the array of atomic point charges without further modification at some distance of the QC[24,26,30,31]. Since the direct-space summation of (1) converges only slowly with growing M, considerable errors can occur[54,56,57]. This becomes manifest in an oscillatory behavior of the chemical shift tensor eigenvalues at various levels of truncation, which in case of ^{31}P amount to ≈1 ppm even for large clusters in [24] (see Fig. 4c of that work).

In more advanced schemes[19,54,56] this uncertainty is removed with moderately increased computational effort by performing an *Ewald summation*[58], which allows the virtually exact calculation of the electrostatic potential for an ideal ionic crystal. Therefore, the presence of the QC is ignored for a moment so that *all* atomic sites of the crystal are represented by point charges. Then, (1) can be rewritten as

$$V(\mathbf{r}_i) = \sum_{j \in UC}^{N} {\sum_{\mathbf{n}}}' \frac{q_j}{r_{ij,\mathbf{n}}} \quad , \tag{2}$$

where index j runs over the N atomic sites in a unit cell (UC), the direct-space grid index $\mathbf{n} = (n_1, n_2, n_3), n_i \in \mathbb{Z}$ points to all possible unit cells and $r_{ij,\mathbf{n}} = |\mathbf{r}_{ij,\mathbf{n}}|$ is the distance between $\mathbf{r}_i$ and the location of atom j in the UC with index $\mathbf{n}$. The prime behind the sum symbol indicates that terms where $\mathbf{r}_i = \mathbf{r}_j$ have to be dropped. According to Ewald eq. (2) can be decomposed in two parts, one summation still in direct space primarily accounting for near distant charges (first term in (3)) and one summation in reciprocal space, primarily for far distant charges (second term in (3))

$$\begin{aligned} V_{Ewald}(\mathbf{r}_i) \;=\; & \sum_{j \in UC}^{N} {\sum_{\mathbf{n}}}' q_j \frac{\operatorname{erfc}(\eta\, r_{ij,\mathbf{n}})}{r_{ij,\mathbf{n}}} + \\ & \frac{1}{\pi V} \sum_{j \in UC}^{N} q_j \sum_{\mathbf{m} \neq \mathbf{0}} \frac{\exp(-[\pi \mathbf{f}_\mathbf{m}/\eta]^2)}{\mathbf{f}_\mathbf{m}^2} \cdot \cos(2\pi \mathbf{f}_\mathbf{m} \cdot \mathbf{r}_{ij,\mathbf{0}}) \end{aligned} \tag{3}$$

where $\mathbf{m} = (m_1, m_2, m_3)$ is the reciprocal grid index, $\eta \in (0, 1)$ the Ewald convergence parameter†, V the unit cell volume, and $\mathbf{f_m}$ the position vector in reciprocal space. Like the direct sum in (2) the Ewald sum in (3) is infinite, i.e. $\mathbf{m}, \mathbf{n} \rightarrow (\infty, \infty, \infty)$, but it converges quickly when $\mathbf{n}$ and $\mathbf{m}$ are simultaneously increased. The implementations in[19,55] use $\eta = 0.2$, $\mathbf{n}_{max} = (8, 8, 8)$ and $\mathbf{m}_{max} = (5, 5, 5)$ to reach converged results.

Once, the exact Ewald potential $V_{Ewald}(\mathbf{r}_i)$ is obtained according to (3) it has to be incorporated in the quantum mechanical electronic structure (QM) calculation. Currently available QM software cannot handle scalar potential fields directly, but a restricted number of point charges, only. Therefor, a fitting procedure is used to vary a finite set of point charges $q_{j,DS}$ with the potential $V_{DS}(\mathbf{r}_i)$ (subscript DS indicates that a direct summation according to (1) is feasible) so that it reproduces V_{Ewald} in the QC region in an optimal sense, i.e. it minimizes the root mean square deviation

$$\Delta_{rms} = \left(\sum_{i}^{N_r} \left[V_{Ewald}(\mathbf{r}_i) - V_{DS}(\mathbf{r}_i) \right]^2 / N_r \right)^{1/2} \tag{4}$$

Different strategies have been devised for the choice of the check points $\mathbf{r}_i$ and their number N_r [29,54,55]. It seems that each strategy leads to satisfactory (=converged) results provided that the check points are reasonably distributed over the QC region and that N_r is sufficiently large. In the algorithm of Klintenberg *et al.*[55] check points are located at all nuclear positions in a sphere containing the QC region and additionally at a larger number (∼1000) of randomly chosen points in the QC region. Each random point falls in the union of spherical shells with an inner and outer radius of 0.1 and 2.5 Å centered at each non-randomly chosen point or previously chosen random points.

Different schemes have also been suggested for the determination of the number and the position of the fitting point charges $q_{j,DS}$. The schemes presented in[54,55] seem to be equally suitable because a converged $V_{DS}(\mathbf{r}_i)$ in the QC region can be obtained with both of them when the number of fitting charges is sufficiently large. Klintenbergs algorithm offers the advantage that it keeps the picture of point charges as classical substitute for atomic sites. This is achieved by *(i)* locating fitting charges only at nuclear positions, *(ii)* freezing the fitting charges near to the QC to the ideal atomic charge values of the infinite crystal, and *(iii)* fitting the remaining charges under the constraint of a minimum norm solution, i.e. with as less deviation from ideal charges as possible.

More significant differences appear in the choice of atomic charge values q_j attributed to the crystalline sites in (3). It should be noted in advance that atomic charges in molecules or crystals are no quantum mechanical observables, so that each quantification is related to an underlying model. In other words, there is no 'true' atomic charge that can be assigned to a q_j and all choices are somewhat arbitrary. Even if a set of charges was available that created the quantum mechanically exact electrostatic potential[59], the electrostatic approximation in the embedded cluster *ansatz*, i.e. the neglect of exchange and correlation interactions, would still prevent an exact description

† η defines the relative weight of the direct space to the reciprocal space sum

of the quantum system. Nevertheless, a few comments can be made on the usefulness of certain choices for q_j which have been used in the past:

1. *Formal oxidation numbers*[26,29,54,55,60] (or *Evjen charges*[31,61–63] as a variant of formal atomic charges) are easy to determine *a priori*. Their usage is inadvisable, however, as the potential resulting from such charges is inaccurate[25]. All tools for wave function analysis indicate that formal charges tend to largely exaggerate the charge separation in ionic systems.

2. *Parametrized atomic charges*[64], e.g. those from molecular mechanics (MM) force fields, certainly pose an improvement over formal oxidation numbers, but have the drawback that they must be determined in advance on suitable reference systems. Formally, empirical parameters are introduced in the cluster calculation.

3. *Mulliken charges*[65] are one of the simplest methods to transfer results of a wave function analysis to embedding charges and have been used, e.g., in[25]. The drawback of Mulliken charges are *(i)* the equal partitioning of atomic overlap populations, which is problematic for ionic systems, *(ii)* the neglect of intra-atomic charge distribution, and *(iii)* the large basis set dependence which is especially problematic for extended or unbalanced basis sets[66]. The basis set dependence is inherent to all basis set related methods of wave function analysis, but can be significantly reduced (see next item).

4. *NBO charges*[66] are obtained from a *natural population analysis* (NPA) which belongs to the class of basis set related methods, too, but shows a number of improvements over Mullikens analysis. NPA takes place in an orthonormal, natural atomic orbital set (NAO) which avoids the partitioning problem of overlap populations and reduces the basis set dependence significantly. Population analyses based on similar ideas have already been presented in earlier works[67–69]. The computational effort to obtain NBO charges is moderate. With these properties NBO charges seem to be a good choice for embedded cluster calculations in ionic systems, where the AO basis is often unbalanced. NBO charges have been used in the EIM approach[19].

5. *ESP derived charges* are designed to mimic the quantum mechanically exact molecular electrostatic potential (ESP)[59] at certain check points $\mathbf{r}_k$ in space as closely as possible. ESP charges depend on the choice of $\mathbf{r}_k$ for which a number of different selection schemes have been proposed[70–75]. In all the schemes the check points are placed "outside of the molecule", near its *van-der Waals* surface. The computational effort for ESP charges is usually moderate.

   Although ESP charges seem to be ideally suited for the representation of an electrostatic embedding potential there are a few well known problems[75]: *(i)* ESP charges are highly sensitive to the molecular conformation, *(ii)* ESP charges

from early implementations are not rotationally invariant[74], i.e. they depend on the orientation of the molecule in the coordinate system, *(iii)* ESP charges of atoms buried in the inner part of the cluster cannot be determined unambiguously in many cases because the fitting procedure in general is statistically under-determined and the larger the molecule is the fewer charges can be assigned validly. ESP (ChelpG) and NBO charges were compared for eight amino acids in[20]. Similar charge values and nearly identical NMR shielding tensors were reported in most cases.

6. *AIM* charges[76] are appealing because of their physically motivated definition. However, their calculation is computationally rather expensive. To our knowledge AIM charges have not been used in cluster calculations on NMR properties so far.

The methods described in 3-6 can be used for *self-contained* cluster calculations, where atomic charges obtained from a population analysis in the QC are transferred to the embedding point charge array[24]. In this way an *a priori* parametrization procedure for the point charges can be avoided. It should be considered that, in return, a change in the environment will usually have an effect on the wave function and the population analysis. This mutual dependency is solved in the EIM approach[19] by an SCF procedure for the embedding charges (*vide infra*).

Another parameter of embedded cluster calculations is the *quantum cluster charge* q_{QC}, i.e. the sum of nuclear and electronic charges in the QC region, given in multiples of the proton charge e. In our opinion q_{QC} should be clearly distinguished from the total system charge, q_{tot}, defined by q_{QC} plus the sum of embedding point charges. q_{QC} fixes the amount of electrons in the QC region and is usually restrained to integer values that allow closed-shell NMR calculations. q_{tot} may take any value and is restricted only by the requirement that the charge array should produce an accurate Ewald potential in the QC region.

Surprisingly little effort has been put on the determination of proper q_{QC}s so far, although this parameter certainly plays an important role. The importance is indirectly shown in Fig. 2 of [54], which indicates that the error of the lattice potential is correlated with q_{QC}. In the past q_{QC} was derived almost exclusively[†] from the sum of formal oxidation numbers of the constituent QC atoms[19,20,29,54,62,63,77]. This led to highly charged QCs in some cases, like $[Mg_9O_9Mg_{16}]^{32+}$ in [77] or $[NiO_6]^{10-}$ in [63]. We like to emphasize that QC charges derived in this way must be regarded as inadequate in the same way as formal charges are inadequate for representing atomic point charges (see above). It seems that most workers intuitively avoided high q_{QC}s by a different cluster construction. However, lower q_{QC}s were accepted in nearly all previous works. For q_{tot} there seems to be a broader agreement that it should be zero[19,20,27,29,62,63]. To the best

[†] An exception is described in [27], where the charge of a $[TiO_5]$ cluster has been reduced from the formal value -6 to -4. The latter value was motivated by the sum of Mulliken atomic charges ($= -4.147$) determined in a periodic calculation and by the requirement of a closed shell calculation.

of our knowledge there are no systematic investigations on how q_{QC} and q_{tot} influence the quality of calculated NMR parameters.

As last criterion for a classification of embedded cluster methods we mention the *modelling of the QC boundary region*. In the simplest setup no special care is taken about the boundary so that QC and point charges are in immediate neighborhood[19]. The abrupt transition is problematic, however. While the electrostatic approximation is acceptable for long distant interactions, say > 5Å for non-bonded atoms[78], it breaks down at smaller distances where quantum effects like chemical bonding and Pauli repulsion between electrons take place. Yudanov *et al.* demonstrated that point charges at the boundary can lead to a significant, unwanted distortion of the QC electron density[77]. The effect is especially pronounced when easily polarizable anions represented by diffuse basis functions in the QC adjoin to positive point charges in the embedding array. An improved description of the ESP at near distances was achieved by expanding the point charge to a charge distribution or multipoles[25,27,78,79]. Further improvement can be achieved, in principle, by replacing the point charges at the boundary with suitable total ion model potentials (TIMPs) that account also for effects of covalent bonding and cluster/environment orthogonality[26,28,31,77]. The TIMPs have to be adapted to the individual bonding situation, however.

Another possibility to account for covalent bonding at the QC boundary is to saturate the dangling bonds with monovalent atoms (usually hydrogen). The technique has frequently been used in QM/MM and ONIOM approaches[80,81] even though not specifically with respect to NMR property calculations in ionic solids. Several aspects of this strategy are problematic: *(i)* a systematic improvement is difficult as the saturated QC formally describes a new quantum system with wrong composition, *(ii)* the charge array has to be modified near the positions where the monovalent atoms are added but there is currently no well-grounded recipe how this can be done, *(iii)* the positioning of the monovalent atoms is unclear. Empirical rules are usually introduced which is unsatisfactory from a theoretical point of view.

Finally, frozen localized orbitals placed at the QC boundary, that are excluded from the SCF procedure, are another possibility to approximate covalent bonding in the cut-off region[82,83]. Like the TIMP and the dangling bond saturation schemes this approach is not self-contained and introduces additional empirical parameters that have to be determined *a priori*.

The probably best but most expensive option is to increase the cluster size so that the boundary will be shifted farther away from the nuclei of interest. This strategy has been pursued in the EIM/cluster approach[20]. Local approximation methods may be introduced to reduce the computational effort for growing QC sizes[84].

A medium course between cluster expansion, local approximation and effective embedding potential was presented recently with the *frozen-density embedding* (FDE) method adapted for NMR calculations by Jacob and Visscher[85], where NMR shieldings are calculated in a subsystem within the QC. The idea of partitioning the QC in further subsystems and keeping the density in parts of them fixed has already been used in earlier calculations on other properties, see[86] and references cited therein.

In our overview we left out general aspects of NMR calculations on molecules such as the choice of the quantum chemical model, the type of the basis set and the choice of gauge for the magnetic shielding calculation. Excellent reviews are available on these topics[9,87]. It is widely accepted now that reliable calculations of NMR parameters require inclusion of electron correlation as well as extended basis sets of at least valence triple-ζ quality plus polarization functions. Diffuse functions are usually unnecessary in solid state calculations because each atom is surrounded by other atoms which provide additional basis functions. The choice of gauge origins by the GIAO method[88] has proven to be satisfactory while being comparably easy to implement for various quantum chemical models.

3 Systematic improvement of a cluster approach

For improved cluster calculations we must eliminate the disadvantages D1–D4 enumerated above as far as possible, while preserving the advantages A1–A5. Nothing can be done to fix the translational symmetry loss (D1), since this is the nature of the cluster approach. In many cases it is beneficial however to preserve local symmetry elements near the nucleus of interest, because they can reduce the computational expense or restrict the shielding tensor orientation. Concerning D2 we prefer an approximate treatment over a complete neglect of long range interactions, which is a compromise between accuracy and expense of the calculation. Concerning D3 we can improve the boundary conditions by requiring certain conditions (see below) for a properly chosen cluster. Looking at our classification scheme in Fig. 1 we find that following the branches on the right side lead to more satisfactory results. Finally, concerning D4 we suggest a systematic way for the cluster generation and provide necessary tools for an automatized setup.

Most NMR cluster calculations presented in the past suffer at least from one of the disadvantages D2–D4 and could be improved at modest additional expense. In the Embedded Ion Method (EIM) and the EIM/cluster method developed by Stueber, Grant and others[1,19,20] a major step is taken towards an improved description of long range interactions (i.e. curing D2) by performing an *Ewald summation* of NBO or ESP charges. Therefore we took this method as a starting point of our work. The heart of the EIM and EIM/cluster approaches is a SCF procedure for the embedding charges which we adopt with modifications that are described in section 3.1. In section 3.3 we use exemplary calculations on NaF to demonstrate the shortcomings of EIM with respect to D3 and D4. We make proposals how these can be cured or at least reduced. To distinguish the traditional EIM from the modified version we will call the latter the *extended embedded ion method* (EEIM).

3.1 SCF procedure for embedding charges (EIM)

The Embedded Ion Method (EIM) combines high-level calculations of a QC including the nuclei of interest with an embedding of the QC in an exact, self-consistent, purely classical electrostatic potential of the crystal field. The expensive part in EIM calculations is usually the QM part, whereas the derivation of the electrostatic potential is relatively cheap. A flow chart of our implementation is given in Fig. 2.

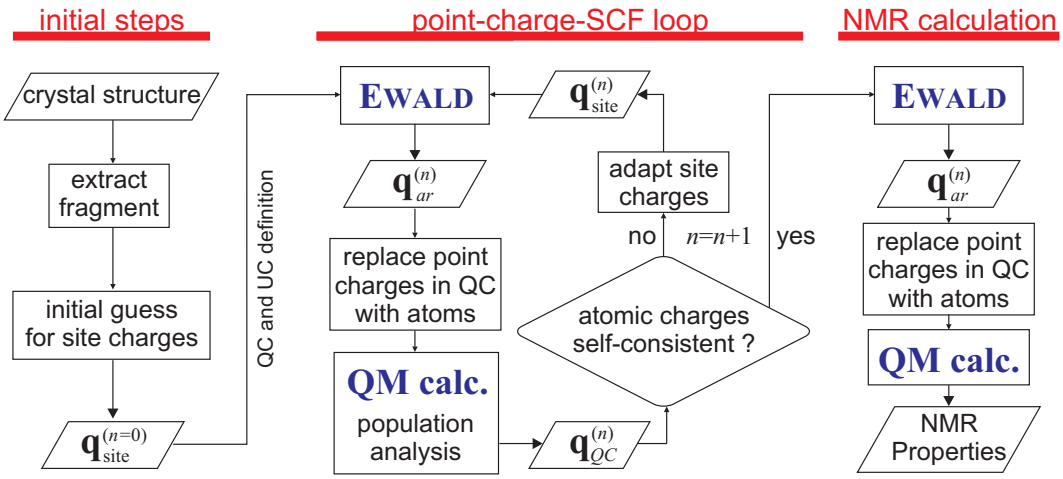

Figure 2: Flowchart of the (E)EIM procedure. (UC: unit cell, QC: quantum cluster, $\mathbf{q}_{site}^{(n)}$: vector of atomic site charges in n-th loop cycle, $\mathbf{q}_{ar}^{(n)}$: charges of embedding array, $\mathbf{q}_{QC}^{(n)}$: atomic charges in QC from population analysis.)

The implementation in this work was made independently from the earlier one reported by Stueber *et al.*[19]. The functionalities of the two implementations are very similar, with the main difference occurring in the initial steps. We therefore give only a short description here, introduce the important input parameters and mention specific modifications.

In the initial steps a suitable fragment of the crystal is chosen as QC and a charge q_{QC} has to be assigned to it. While the traditional scheme[19] proceeds with an electronic structure calculation on the non-embedded QC in order to obtain an initial set of atomic site charges ($\mathbf{q}_{\mathrm{site}}$), we prefer a simple initial guess for $\mathbf{q}_{\mathrm{site}}$ at the beginning, so that the first QM calculation is already performed on an embedded QC. We believe that this adds more robustness to the scheme, as we observed convergence problems in several electronic structure calculations on non-embedded QCs, whereas no problems were present when the same QCs were embedded[†]. Moreover, making a reasonable guess instead of an initial QM calculation reduces the computational effort. By default we use formal atomic charges for the initial site charges. In the next step we enter the

[†] In this work we leave out the partial structure optimizations described for non-embedded QCs in[19]. Partial optimizations can also be performed in the presence of point charges[21], but special precautions have to be met in order to make them reasonable.

point-charge-SCF loop (see Fig. 2, not to be confused with the SCF procedure in the electronic structure calculation).

From the unit cell definition and the atomic site charges the EWALD program creates a finite point charge array, $\mathbf{q}_{ar}$, that mimics the lattice potential of an ideal (infinitely extended) crystal in a region enclosing the QC. The program is based on the code of Klintenberg *et al.*[55] with modifications similar to those described in[19].

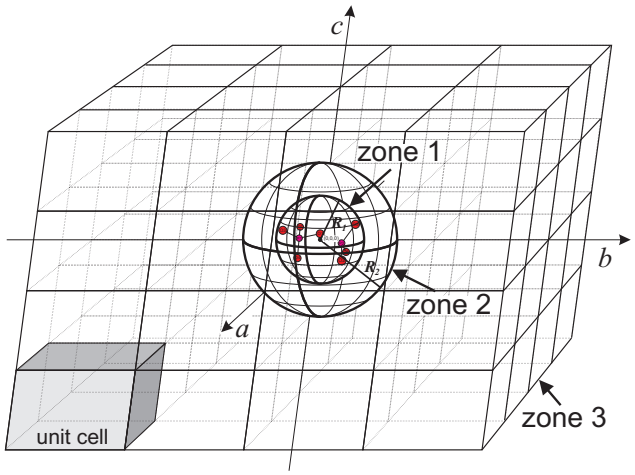

Figure 3: Definition of the three zones in the (E)EIM procedure.

The finite point charge array is composed of three disjoint zones as shown in Fig. 3. Assume the QC consists of N_{QC} atoms. Zone 1 is a spherical volume with the minimal radius R_1 around the origin (0,0,0) that contains all QC atoms. The number of atoms in zone 1 is $N_1 \geq N_{QC}$ and typically amounts to $\sim 10^2$. R_1 and N_1 are determined through the QC definition. Zone 2 is a spherical shell around zone 1 containing N_2 atoms (typically, $\sim 10^2$–10^3). A lower bound of $N_1 + N_2$ has to be given as input parameter. Since all atoms with equal distance from the origin should be gathered in the same zone the actual N_2 is determined by the next higher number in a spherical shell expansion that fulfills this criterion. R_2 is the final outer radius of zone 2. The atoms of zones 1 and 2 are described by unaltered input charges. Zone 3 is a parallelepiped enclosing zone 2 and is generated by replicating the unit cell at (0,0,0) N_a times along the positive and negative direction of crystallographic axis **a**, N_b times along $\pm\mathbf{b}$, and N_c times along $\pm\mathbf{c}$ (N_a, N_b, $N_c \sim 6$, typically). If N_{UC} is the number of atoms per unit cell, zone 3 contains $N_3 = (2N_a \times 2N_b \times 2N_c) \times N_{UC} - N_2 - N_1$ atoms (typically $\sim 10^5$). The atoms of zone 3 are substituted by fittable charges in order to mimic the exact lattice potential in zone 1 and 2. The direct sum potential of the point charge array is

$$V_{DS}(\mathbf{r}_i) = \sum_j{}' \frac{q_j}{r_{ij}} \text{ with } j \in \text{zones 1, 2, 3} \tag{5}$$

Each zone 3 charge may be varied independently. The fitting procedure minimizes Δ_{rms} defined in eq. 4 under the following constraints: *(i)* the total charge q_{tot} must be

zero, *(ii)* the dipole moment of the point charge array must be zero, *(iii)* among various sets of zone 3 charges that might minimize Δ_{rms} under the previous constraints the one is chosen where the sum of charge deviations from the corresponding input charges is minimal ("minimum norm solution"). The set of checkpoints $\mathbf{r}_i$ at which the potential is calculated consists of all atomic positions in zone 1 and 2 as well as a number of N_{rcp} randomly chosen interstitial points in zone 1. N_{rcp} has to be given as input parameter and is typically chosen two to four times $N_1 + N_2$. In a first step the exact Ewald potential according to eq. 3 is calculated at the $N_r = N_1 + N_2 + N_{rcp}$ checkpoints. Then, the charge fitting is performed by solving the system of $N_r + 4$ linear equations defined in[55] (equations 6 to 10). At this step we improved the program efficiency by replacing the default solver routine `dgelsx` from the LAPACK library[89] by vendor specific, CPU optimized implementations[90,91]. The final charge array is considered as a reasonable approximation to the lattice potential if $\Delta_{rms} < 10\mu\mathrm{V}$[20], and if the fitted charges vary by less than 0.1 from the charges in zone 1 and 2.

The optimized point charge array, $\mathbf{q}_{ar}$, is written to a file with an appropriate input format for the subsequent electronic structure calculation. The charge points in the QC region are replaced by quantum mechanically defined atoms consisting of a nucleus and electrons in orbitals. In principle, any electronic structure program may be used that *(i)* can do SCF calculations in presence of a large number of point charges, *(ii)* is able to do a reasonable population analysis and *(iii)* is able to calculate the desired NMR parameters. In this work the GAUSSIAN 03 package was used. Typically, we employ a hybride DFT model and triple-ζ AO basis sets with multiple sets of polarization functions. Atomic charges within the QC, $\mathbf{q}_{QC}$, are determined by NBO population analysis.

Resulting NBO charges $q^{(n)}_{QC,i}$ of the i-th atom in the n-th point-charge-SCF cycle are compared with the NBO charges $q^{(n-1)}_{QC,i}$ of the previous cycle ($\forall n : \sum_i q^{(n)}_{QC,i} = q_{QC}$). In our definition self-consistency of the point charges is achieved when

$$\epsilon = |q^{(n)}_{QC,i} - q^{(n-1)}_{QC,i}| \leq 10^{-5} \text{ for all } i \tag{6}$$

in units of the proton charge $e(= 1.602\times10^{-19}C)$. This convergence criterion is stricter than the one given in[19]; in contrast to former investigations on the charge convergence we optimize *all* site charges in this work and we therefore wanted to minimize the error from this source as far as possible. If self-consistency is not achieved the NBO charges are transferred to the atomic site charges (input for EWALD) and the next SCF cycle is performed. If the convergence criterion is fulfilled (usually happens in less than 15 cycles) the program exits the point-charge-SCF loop, creates the final point charge array by an additional EWALD run and performs the NMR calculation using the GIAO method[88].

3.2 Problems of the EIM approach

In the past the EIM was mainly applied to organic compounds with relatively low ion charges. In the following we will enumerate some conceptual deficiencies or open questions of the EIM that gain importance when typical inorganic compounds with highly charged ions are involved. We will show how these problems can be avoided or reduced.

1. **Dependency on formal charges.** It is clear (cf. section 2) that formal atomic charges should be avoided in embedded cluster calculations. The EIM does not follow this guideline strictly. Although NBO charges are used for charge partitioning within the QC, the total QC charge itself is still determined *a priori* by summing up the formal charges of the constituent atoms. Moreover, formal charges are assigned to crystallographic sites that have no representative in the QC[19,92]. All this can lead to methodological inconsistencies as well as to a pronounced charge mismatch, especially in the treatment of highly charged ions.

2. **Lack of generality.** An important aspect of the EIM or EIM/cluster approach, which – to our knowledge – has not been discussed in detail so far, is the transfer of the NBO charges to the embedding charges (step "adapt site charges", $\mathbf{q}_{QC}^{(n-1)} \rightarrow \mathbf{q}_{\text{site}}^{(n)}$ in Fig. 2). In the following we show that a consistent transfer implies a restricted choice of QCs.

   Let us assume a scenario where a certain crystallographic site is present for multiple times in the QC. Because a symmetry loss can occur in the cluster approach, population analysis can yield different atomic charges for that site. It is then unclear which of the charges should be transferred to the embedding field. Selecting one of the charges arbitrarily will in general lead to the unreasonable result that the total unit cell charge and the total embedding field charge is unequal zero. Without extension the EIM is strictly only applicable to QCs which contain each crystallographic site at most for one time.

   Furthermore, it has been claimed that the traditional EIM or EIM/cluster approach cannot be applied to crystals composed of covalent networks[1]. This comes from the requirement that the QC has to be a finite, closed shell molecule with integer charge calculated from the atomic formal charges.

3. **Lack of systematic improvement.** The traditional EIM approach defined the QC as the molecule containing the nuclei of interest, i.e. a set of only covalently bound atoms like the complex anions in[19,92]. This definition left no space for systematic improvements. In order to obtain more accurate results the QC has to be extended and the electrostatically treated part must be reduced. The advantage of an extended QC has been recognized in the EIM/cluster approach[20] but the composition of the QCs still seems not well formalized. From a fundamental point of view, a systematic improvement of the cluster approach can only be achieved, when the QC adapts more and more the characteristics of a

macroscopic crystal. Of course this cannot be used as a practical advice, but at least we can try to incorporate certain boundary conditions that define a crystal, such as charge neutrality, at every stage of our approximation.

The effect of the deficiencies is demonstrated with a few simple calculations: We calculate the ^{19}F chemical shift parameters of solid sodium fluoride (NaF) at mPW1PW/6-31G(d,p) level with non-embedded cluster, EIM and EIM/cluster calculations. Details of the conversion from the absolute shielding scale to the chemical shift scale are given in section 4. Good results should be near the experimental values $\delta_{iso}^{^{19}F} = -221$ ppm[93] and $\delta_{aniso}^{^{19}F} = 0$ ppm. The latter value results from the fact that the fluorine atoms are located on O_h symmetric sites in an ideal NaF crystal[94]. Several QCs that may be chosen are shown in Fig. 4.

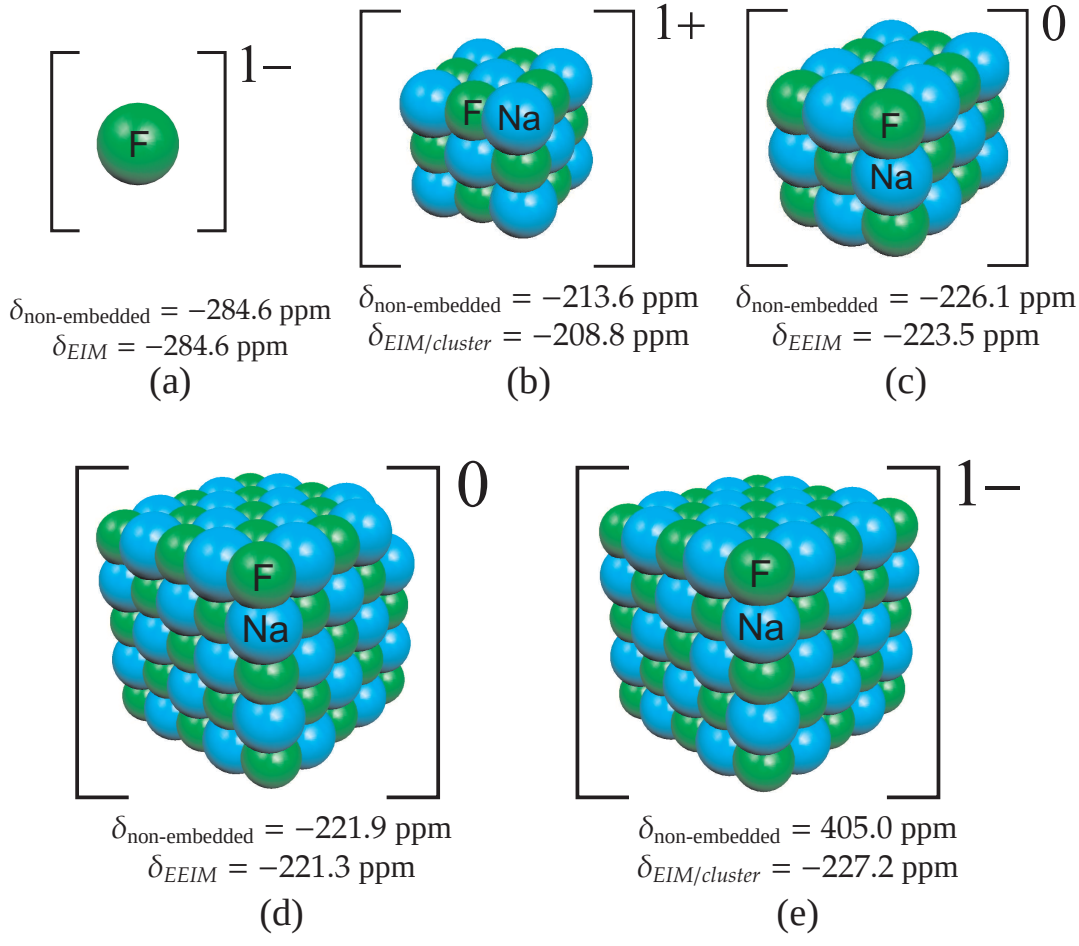

Figure 4: Choices of quantum clusters for (E)EIM calculations of the ^{19}F shielding tensor in sodium fluoride. Fluorine atoms drawn in green, sodium in cyan. (a) F^-, (b) $[Na_{14}F_{13}]^+$, (c) $[Na_{18}F_{18}]^0$, (d) $[Na_{62}F_{62}]^0$, (e) $[Na_{62}F_{63}]^{1-}$. The given chemical shifts always refer to the F^- nucleus closest to the center of the corresponding cluster.

The first QC (Fig. 4a) consists of a single fluorine anion only. This choice follows the guidelines of the classical EIM, in which the bare anion is chosen as QC. The QC charge q_{QC} is fixed to -1 according the formal charge of F^-. Once fixed, the EIM does not alter q_{QC} any more, but merely redistributes partial charges between the atoms within the QC. This has no effect in case of a single atom and, hence, all parameters of this EIM calculation are determined by formal charges: A charge of -1 is transferred to the embedding point charges at fluorine sites and a charge of +1 is assigned to the Na sites in order to achieve charge neutrality. The resulting EIM shift $\delta_{iso}^{^{19}F} = -284.6$ ppm is significantly smaller than the experimental value and does not differ from the value of the corresponding non-embedded calculation. Obviously, the too strong shielding results from an excess of electron density in the QC that cannot be removed by the embedding charge field.

The second QC ($[Na_{14}F_{13}]^+$, Fig. 4b) seems to represent a possible choice for an EIM/cluster calculation. q_{QC}=+1 is again obtained from formal charges. However, a consistent charge distribution with a total cluster charge q_{tot}=0 and unit cell charge q_{UC}=0 is achieved only as long as formal charges are assumed for the atomic charges in the QC and in the point charge array. Starting the point-charge-SCF loop of the EIM leads to inconsistencies: The NBO charge of the QCs' central F-atom (-0.87) differs from the NBO charges of the edge centered F-atoms (-0.89), so that it is unclear what charge should be transferred to the F-sites of the point charge array. An analogous problem arises for the Na-sites because of different NBO charges of Na-atoms at the face centers (0.84) and at the corners (0.93) of the QC, respectively. Selecting any pair of these unmodified F and Na NBO charges leads to the unphysical result $q_{tot} \neq 0$ and $q_{UC} \neq 0$. The latter inequality is also incompatible with the requirements of the EWALD program. Assigning averaged site charges of the kind

$$\bar{q}_F^{(n)} = \tfrac{1}{13} \sum_{j=1}^{13} q_{QC,F_j}^{(n-1)} \quad \text{and} \quad \bar{q}_{Na}^{(n)} = \tfrac{1}{14} \sum_{k=1}^{14} q_{QC,Na_k}^{(n-1)} \tag{7}$$

does not solve the problem, because $\bar{q}_F \neq -\bar{q}_{Na}$ is obtained for this cluster, which would yield again $q_{UC} \neq 0$. A possibility to restore charge neutrality for the unit cell is to define atomic charges as

$$\tilde{q}_F^{(n)} = \tfrac{1}{2}(\bar{q}_F^{(n)} - \bar{q}_{Na}^{(n)}) \quad \text{and} \quad \tilde{q}_{Na}^{(n)} = \tfrac{1}{2}(\bar{q}_{Na}^{(n)} - \bar{q}_F^{(n)}) \tag{8}$$

This allows a pseudo EIM procedure in which $q_{tot} \neq 0$ after the replacement step of point charges in the QC region with atoms (see Fig. 2). In other words, there is a charge mismatch between q_{QC} (=+1) and the sum of the replaced point charges which makes the procedure inconsistent. Nevertheless, eq. 6 provides an abort criterion for the point-charge optimization cycle. The final pseudo EIM charge amounts to $\tilde{q}_F^{(3)} = -0.86864 = -\tilde{q}_{Na}^{(3)}$ with a charge mismatch of $q_{QC} - 0.86864 = 0.13136$. The calculated isotropic shift for the central F nucleus amounts to -208.8 ppm. The deshielding of 12.2 ppm with respect to the experimental value is in parts probably

also an effect of the electron deficiency in the QC[†]. The effect of the QC charge mismatch on $\delta_{iso}^{^{19}F}$ becomes more clear in the series of pseudo EIM/cluster calculations using $[Na_{14}F_{13}]^X$ QCs with different cluster charges $X = \{-3, -1, +1, +3\}$. The results are shown in Fig. 5 and confirm the expected trend from a simplistic view that positively charged QCs yield too large $\delta_{iso}^{^{19}F}$ values (magnetic shielding too weak) whereas negatively charged QCs yield too small $\delta_{iso}^{^{19}F}$ (shielding too strong). As demonstrated by the shift of $[Na_{14}F_{13}]^{5-}$, there is no simple (monotonic) correlation between X and $\delta_{iso}^{^{19}F}$ in molecules, however, because the changes of $\delta_{iso}^{^{19}F}$ depend primarily on paramagnetic and diamagnetic shielding contributions, whose magnitudes depend in a more complicated way on the electronic structure. In any case, charge mismatches seem to be disadvantageous.

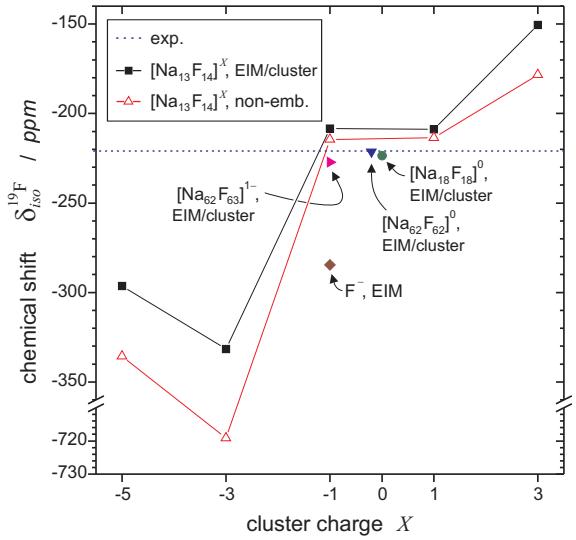

Figure 5: Dependency of $\delta_{iso}^{^{19}F}$(central F-nucleus) on the cluster charge X in embedded and non-embedded quantum clusters $[Na_{14}F_{13}]^X$. Additional data points are given for other EIM/cluster calculations.

The charge mismatch described in the previous paragraph can be avoided by a QC construction with equal amounts of sodium and fluorine atoms. In such cases one always obtains $q_{QC} = 0$, $\bar{q}_F = -\bar{q}_{Na}$ and hence $q_{UC} = 0$ as well as $q_{tot} = 0$. The QCs $[Na_{18}F_{18}]^0$ (Fig. 4c) and $[Na_{62}F_{62}]^0$ (Fig. 4d) follow this guideline. The calculated isotropic shifts for the central F-nucleus of -223.5 ppm and -221.3 ppm, respectively, are in excellent agreement with the experimental value. This indicates that uncharged QCs are generally a favorable choice.

[†] Compared to the true electron distribution in an equivalent cutout of the NaF crystal the $[Na_{14}F_{13}]^+$ cluster has an electron deficiency, because formal atomic charges are always an exaggerated description of the true charge distribution between anions and cations.

A drawback of $[Na_{18}F_{18}]^0$ is the loss of O_h symmetry, which leads to a dipole moment of the QC[†], a spurious electric field gradient (EFG) unequal to zero at the central F-nucleus, and a chemical shift anisotropy of $\delta_{aniso} = -13.5$ ppm. It is clear that no finite QC can be realized for NaF where both charge and the next higher electrical moment are zero. A reasonable compromise has to be met. Improvement can be achieved by moving the QC boundary farther away from the nucleus of interest, while keeping the charge mismatch and the EFG small. In $[Na_{62}F_{62}]^0$ the anisotropy of the central ^{19}F nucleus reduces to $\delta_{aniso} = -8.1$ ppm[‡]. O_h symmetry and $\delta_{aniso} = 0$ ppm is restored in $[Na_{62}F_{63}]^{1-}$ (Fig. 4e). The isotropic shift of the non-embedded calculation shows a large deviation from the experimental value[§] while $\delta_{iso}^{^{19}F} = -227.2$ ppm for the embedded calculation is acceptable.

3.3 The Extended Embedded Ion Method (EEIM)

The problems with the traditional EIM method mentioned in the previous section can be avoided or reduced if the following guidelines for QC construction are taken into account. These constitute the EEIM.

Elimination of the charge mismatch. An improved scheme should not be based on formal charges. This can be accomplished as follows. In spite of the fact that atomic charges are no observables, one exact rule for atomic charges in (ordinary) crystals is always valid: The sum of atomic charges in a unit cell (UC) is zero

$$q_{UC} = \sum_{i \in UC} q_i = 0 \quad . \tag{9}$$

The cell is generally composed of a finite number of different atomic sites X_j ($j = 1, 2, \ldots N$), each of which occurs $M(X_j)$ times in the UC. ($M(X_j)$ is the multiplicity of the Wyckoff symbol for the site.) The relative frequency of a site in the UC is $f_{UC}(X_j) = M(X_j)/\sum_j M(X_j) = M(X_j)/N_{UC}$. Thus, it is possible to construct a QC with an exact charge of

$$q_{QC} = 0 \tag{10}$$

if all different atomic sites are included with the same relative frequency as in the UC

$$f_{QC}(X_j) = f_{UC}(X_j) \text{ for all } j \ . \tag{11}$$

With such a QC, population analysis will give atomic (NBO) charges for *all* sites which can be transferred to the point charge array. The abovementioned dilemma (section 3.2) in the assignment of site charges q_{X_j}, if a site is present for several (n) times

[†] The embedding charges do not fully compensate the dipole moment [‡] Further improvement to δ_{aniso}=+0.4 ppm was achieved when the flexibility of the atomic basis at the cluster boundary of $[Na_{62}F_{62}]^0$ was reduced to a minimal CEP-4G basis. On the other hand, the usage of numerous PPs in the vicinity of the central nucleus introduces a deviation in the isotropic shielding (δ_{iso}=-216.4 ppm). [§] The origin of the deviation is unclear so far but might be related to numerical problems due to near orbital degeneracies.

in a QC with broken symmetry, can be avoided by averaging over the corresponding NBO charges.

$$q_{X_j} = \frac{1}{n} \sum_{i \in X_j}^{n} q_{QC,i} \quad . \tag{12}$$

In case of large unit cells the inclusion of all sites with their correct relative frequency in the QC is not viable anymore. Then, the next best directive is to group subsets of similar atomic sites into *atomic types* Ξ_ν, which have an averaged atomic charge and a joint relative frequency (*atomic grouping*). Several atomic types may be defined at a time but the sets must be disjoint. The relative frequencies of the atomic types must be the same in the QC and the UC, otherwise either q_{QC} or q_{UC} may deviate from zero in the course of the EIM charge optimization. The rules for atomic grouping are summarized in the following equations:

$$\Xi_\nu = \{X_j, X_k, \ldots, X_z\} \quad \text{where} \quad \Xi_\nu \cap \Xi_\mu = 0 \ \text{ for } \ \mu \neq \nu = 1, 2, \ldots \tag{13}$$

$$M(\Xi_\nu) = M(X_j) + M(X_k) + \ldots + M(X_z) \tag{14}$$

$$f_{UC}(\Xi_\nu) = M(\Xi_\nu) / [\sum_{\mu} M(\Xi_\mu) + \sum_{a} M(X_a)] \qquad \text{where } X_a \notin \Xi_\mu \tag{15}$$

$$f_{QC}(\Xi_\nu) = f_{UC}(\Xi_\nu) \ \ \wedge \ \ f_{QC}(X_a) = f_{UC}(X_a) \qquad \text{for all } \nu, a \tag{16}$$

$$q_{\Xi_\nu} = \frac{1}{m} \sum_{i \in \Xi_\nu}^{m} q_{QC,i} \ \ \wedge \ \ q_{X_a} = \frac{1}{n} \sum_{i \in X_a}^{n} q_{QC,i} \ . \tag{17}$$

In this approximation atomic types and ungrouped atomic sites X_a are treated exactly in the same way. Equations 16 and 17 replace the exact conditions 11 and 12, respectively. A good choice for an atomic type is the grouping of two or more sites which contain the same element in the same oxidation state and in a similar coordination environment. The scheme is still independent of formal charges and the charge mismatch relative to the exact treatment (eq. 11) is expected to be small. Thus, more compact clusters may be constructed. An example for atomic grouping in EEIM calculations is given in section 6.1, where we group the two different sites Mg1 and Mg2 in $Mg_2P_4O_{12}$ to the type “Mg”.

The important idea behind the previous directives is that there is a physically motivated reason to prefer $q_{QC} = 0$ in an embedded QC setup – not only q_{tot}=0 as advocated in numerous works. A charged QC more likely has a bigger charge mismatch, which is particularly disadvantageous in an EIM scheme where the mismatch is transferred also to the embedding charges. Another advantage of an uncharged QC is that it does not interact with the embedding field via its zeroth electrical moment. Compared to a charged QC this usually reduces the electrostatic interaction energy, and hence the error portion that is introduced by approximating the quantum mechanical with the classical electrostatic interaction. In some cases it may be impossible to create an uncharged QC. In order to keep the charge mismatch small we recommend to construct QCs with q_{QC} as low as possible, chosen on the basis of atomic charges derived

from population analysis. Without mentioning the physical motivation above, electroneutral QCs were chosen already in several (but not all) EIM/cluster calculations[20,23].

Improvement of the embedding quality. Apart from restoring charge neutrality the benefit of treating a bigger region around the nuclei of interest on a quantum mechanical rather than an electrostatical level is that the inner part of the QC is exposed to an improved potential which includes also exchange interaction. Moreover, insertion of a buffer zone at the QC boundary helps to reduce the artificial distortion of the electron density induced by close contacts between electrons in orbitals and point charges.

Our current strategy is to use a "locally dense basis", i.e. an extended set of AO basis functions in the region where the nucleus with the shielding tensor of interest is located and a (gradually) reduced AO expansion at farther distances. At the QC boundary the AO expansion is usually reduced to minimal, compact basis sets and a PP approximation for the inner shells. The inflexibility of the minimal basis prevents larger artificial distortions and is beneficial with respect to computational resources. Locally dense bases are well established in non-embedded NMR calculations[95,96].

Generalization to networked solids. It has been claimed that the traditional EIM or EIM/cluster cannot be applied to crystals composed of covalent networks[1]. In view of the systematic expansion described above there should be no general problem in calculating such networks. Naturally an error is introduced at the QC boundary where a covalent bond has to be broken. However, if this defect is located at far distance from the nucleus of interest, its effect on the shielding tensor will be small. In section 6.4 we present a calculation on magnesium ultra phosphate, MgP_4O_{11}, in which the phosphate units are part of an infinite network. Problems are expected in networks with electron delocalization, where the defect might not be localized any more. Saturation of the dangling bonds with suitable terminators might give an improvement in such cases.

Formalization of the QC construction. A fixed scheme for QC construction has the advantage, that the quality of the calculation is determined by few parameters and that the results in a series of calculations are better comparable to each other. The crystal structure must be known. Then, we use the following guidelines:

1. A spatial origin $\mathbf{r}_0$ of the QC must be chosen. Often the choice is $\mathbf{r}_0 = \mathbf{r}_X$, i.e. the position of nucleus X for which we intend to calculate the magnetic shielding σ^X. If we want to obtain σ for several nuclei X_1, X_2, ... X_n in one calculation we may choose $\mathbf{r}_0 = \frac{1}{n}\sum_i^n \mathbf{r}_{X_i}$. In case of larger distances $|\mathbf{r}_{X_i} - \mathbf{r}_{X_j}|$ one will usually decide to split the problem in two or more separate QCs.

2. If a point $\mathbf{r}_s$ of higher point group symmetry is present close to $\mathbf{r}_0$ chosen in 1 one might prefer to reassign $\mathbf{r}_0 = \mathbf{r}_s$ in order to create a QC with higher symmetry.

3. The locality of σ^X suggests that the QC should be roughly expanded in spherical shells around $\mathbf{r}_X$. A sphere with radius R around $\mathbf{r}_0$ is filled with atomic sites. Typically, $R = 3.0 - 5.5$ Å so that the second to third coordination sphere around X is complete.

4. Covalent fragments formed in 3 are completed – if possible – in order to avoid dangling bonds in the vicinity of X. Further atoms are added in order to fulfill equations 11 or 16 that assure $q_{QC} = 0$. The QC border line should be drawn between atoms with ionic interactions, since these have less directional character and are therefore expected to be better replaceable by a point charge interaction.

5. The cartesian coordinates of the QC (and the fractional coordinates of the UC) are translated so that $\mathbf{r}_0 = (0, 0, 0)$. This is required by the `Ewald` program, see section 3.1.

6. A quantum chemical method and a locally dense basis have to be chosen, which are able to describe the wave function in the region of the nuclei of interest with sufficient accuracy. In many cases electron correlation needs to be considered. Currently, we favor hybride DFT due to its good cost/performance ratio.

   The creation of a locally dense AO set is based on a distance criterion from a reference point. In our implementation, K different reference points $\{\mathbf{r}_{ref,k}\}$ ($k = 1, 2, \ldots K$) may be defined simultaneously. A common choice is $\{\mathbf{r}_{ref,k}\} = \{\mathbf{r}_{X_i}\}$. Then, M different radial shells with a shell range $r_m \in [r_{min,m}, r_{max,m}[$, ($m = 1, 2, \ldots M$, $r_{max,m} \geq r_{min,m+1}$) are defined around each $\mathbf{r}_{ref,k}$. Atoms located in the different shells form disjoint sets[†] and for each set an AO basis definition is given. By default the basis definition applies to all atoms of the shell, but a restriction to certain atom types is possible,too. Pseudopotentials can be assigned in the same manner.

   An AO set of valence triple-ζ quality plus a double set of polarization functions should be considered as minimum requirement for the innermost shell ($m = 1$), which contains the nuclei $\{X_i\}$ of interest and usually their nearest bonding partners. The use of pseudopotentials in this region should be avoided. For shells with higher m the basis set quality is reduced. Compact AOs are advisable at the QC boundary. For example, Fig. 6 shows the shell and basis definition for the EEIM calculation on the $[Mg_2P_4O_{12}]_3$ cluster (discussed in more detail in section 6). The nearest distance relative to one of the four central P atoms decides upon the basis set assignment. Below 2.0 Å a 6-311G(3df,3pd) basis is assigned, from 2.0 up to 4.7 Å a 6-31G(d,p) basis, and for distances equal or larger 4.7 Å a CEP-4G basis with corresponding pseudopotentials, supplemented by a d-function for each P atom.

[†] If $K > 1$ each point $\mathbf{r}$ in space is assigned to a specific reference point $\mathbf{r}_{ref,k}$ for which $|\mathbf{r} - \mathbf{r}_{ref,k}| = \min$.

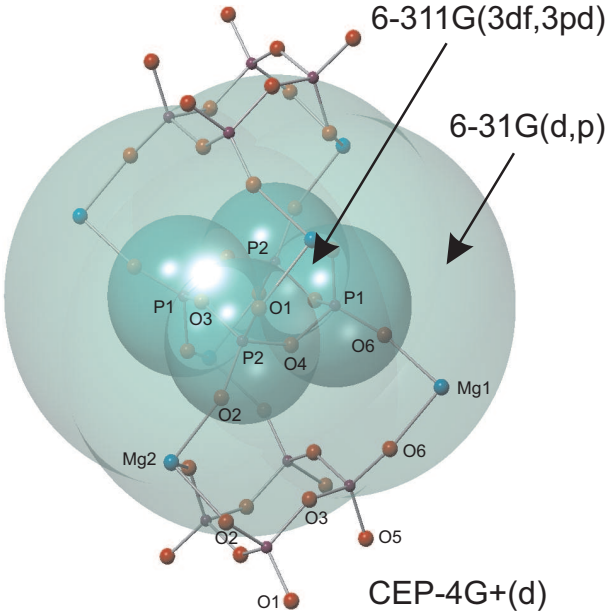

Figure 6: Automated assignment of AOs and PPs in spherical regions around ^{31}P atoms in the $[Mg_2P_4O_{12}]_3^0$ cluster (Mg: cyan, P: magenta, O: red). Innermost region: 6-311G(3df,3pd) basis, second region: 6-31G(d,p) basis, remaining part: CEP-4G+(d) AO+PP set.

4 Computational Details

General information. The DIAMOND (ver 2.0h) program[97] was used to extract suitable quantum clusters (QCs) from the crystal structures. The program permits the filling of spherical shells around arbitrary centers and automatic completion of covalently bound fragments. QC and unit cell (UC) information is exported in fractional coordinates to separate files. A file for the automatized setup of a locally dense basis is created that contains reference points, radial shells and basis set definitions.

A collection of shell scripts and small Perl programs[98] then prepares input files for EWALD and the electronic structure program. In a first step the fractional coordinates of the UC and the QC are translated in order to locate the nuclei of interest near the origin. Second, the fractional QC coordinates are transformed to cartesian ones via

$$\mathbf{r}_{fract.coord}.\overleftrightarrow{T} = \mathbf{r}_{cart.coord} \quad . \tag{18}$$

The transformation matrix $\overleftrightarrow{T}$ from fractional to cartesian coordinates is determined

from the unit cell parameters a, b, c, α, β, γ according to[99]

$$\overleftrightarrow{T} = \begin{pmatrix} a & 0 & 0 \\ b\cos(\gamma) & b\sin(\gamma) & 0 \\ c\cos(\beta) & \frac{c(\cos(\alpha)-\cos(\beta)\cos(\gamma))}{\sin(\gamma)} & \frac{V}{a\cdot b\sin(\gamma)} \end{pmatrix} \tag{19}$$

$$\text{with } V = a\cdot b\cdot c\cdot\sqrt{1-\cos^2(\alpha)-\cos^2(\beta)-\cos^2(\gamma)+2\cos(\alpha)\cos(\beta)\cos(\gamma)} \tag{20}$$

Third, input files for the electronic structure program are generated which define the QC with a locally dense basis and the initial embedding charge field. The master program for the EEIM SCF procedure shown Fig. 2 is a shell script in order to allow flexible user interaction on compute clusters with queueing systems.

All electronic structure calculations were performed with the GAUSSIAN 03 package[41]. The hybride density functional mPW1PW[100] was used throughout with tight convergence criteria for the SCF, corresponding to maximum deviations in density matrix elements of 10^{-6} and in the energy of 10^{-6} Hartree. Quadrature in the DFT calculations was performed on a pruned grid of 99 radial shells and 590 angular points per shell on each atom. Absolute nuclear magnetic shielding tensors $\overleftrightarrow{\sigma}$ were obtained with the GIAO formalism[88]. Atomic charges were obtained by NBO population analysis[101].

Calculations on NaF. The $Fm\bar{3}m$ symmetric crystal structure data was taken from[102] as published in the ICSD database[103]. The Na-F distance amounts to 2.307 Å. Selected clusters are shown in Fig. 4. Calculated ^{19}F chemical shifts are given according to IUPAC recommendations[104] on a scale relative to the reference compound $CFCl_3$

$$\delta = \frac{\nu-\nu(\text{ref})}{\nu(\text{ref})} = \frac{\sigma(\text{ref})-\sigma}{1-\sigma(\text{ref})} \approx \sigma(\text{ref})-\sigma \tag{21}$$

but we used gaseous hydrogen fluoride (HF) as secondary reference. The gas-phase structure (r_g(H-F)=0.9169 Å) was taken from[105]. The experimental gas-phase shift of $\delta_{exp.}$(HF)=-221.34 ppm was reported in[106]. Conversions from the absolute shielding scale to the chemical shift scale were performed by

$$\delta^{^{19}F}_{calc.} = \sigma^{^{19}F}_{calc.}(\text{HF}) - \sigma^{^{19}F} + \delta^{^{19}F}_{exp.}(\text{HF}) \tag{22}$$

Calculations performed at mPW1PW/6-31G(d,p) level are certainly not accurate enough to predict ^{19}F shifts reliably within 1 ppm (, which is seemingly suggested by the presented results). As we were mainly interested in the relative shifts between various clusters the level seems to be sufficient, however.

Calculations on magnesium phosphates. Experimentally determined crystal structures[107–110] were used for the calculations without further structural optimization. Clusters were constructed according to the guidelines given in section 3.3 with locally dense basis sets defined by radial shells around the nuclei of interest (see section 3.3). Basis functions of the 6-311G(3df,3pd) set[41,111–113] were used for the innermost shell, functions of the 6-31G(d,p) set[114–116] for the second shell (if present) and functions of

the CEP-4G set with pseudopotentials[117] for the third shell (if present). The CEP-4G set of phosphorus was supplemented with a *d*-function from the 6-31G(d,p) set (gaussian exponent = 0.55 a_0^{-2}). Calculated ^{31}P chemical shifts are given according to[104] by eq. (21) with 85% H_3PO_4 as reference compound. The computational treatment of this reference is difficult, however. Therefor we assumed a linear relation between quantum chemically calculated magnetic shieldings and experimental ^{31}P chemical shifts

$$\sigma_{calc.}^{^{31}P} = A + B \cdot \delta_{exp.}^{^{31}P} \quad . \tag{23}$$

The parameters $A = 303.29\,\text{ppm}$ and $B = -1.1174$ were determined from a least squares fit of 23 calculated and experimental data from 19 small phosphorus molecules that cover the whole ^{31}P isotropic chemical shift range. The fit had a standard deviation of $SD = 9.56\,\text{ppm}$. Calculations were performed on mPW1PW level with 6-311G(3df,3pd) basis functions at all centers. Experimentally determined molecular structures were used in order to account for vibrational effects. Solving eq. (23) for δ gives the final expression used for the calculation of isotropic chemical shifts and shift tensor eigenvalues

$$\delta_{ii,calc.}^{^{31}P} = \frac{\sigma_{ii,calc.}^{^{31}P} - 303.29\,\text{ppm}}{-1.1174} \quad , \quad i = 1,2,3 \tag{24}$$

At mPW1PW/6-311++G(3df,3pd) level the optimized parameters were $A = 302.99\,\text{ppm}$, $B = -1.1147$ ($SD = 9.88\,\text{ppm}$) and at mPW1PW/6-31G(d,p) level $A = 371.87\,\text{ppm}$, $B = -1.0058$ ($SD = 17.25\,\text{ppm}$). More details on the fits are given in the supplemental material.

5 Experimental Details

Synthesis. The educts magnesium orthophosphate octahydrate ($Mg_3(PO_4)_2 \cdot 8\,H_2O$), magnesium hydrogen phosphate trihydrate ($MgHPO_4 \cdot 3\,H_2O$), and diammonium hydrogen phosphate ($(NH_4)_2HPO_4$) were obtained from cfb Budenheim (Budenheim, Germany). P_4O_{10} was obtained from Riedel-de-Haën (Seelze, Germany). Unless noted otherwise the reactions were carried out in an open, Y_2O_3-stabilized ZrO_2 crucible placed in a tube furnace with temperature sensor and external heat program controller.

Synthesis of α-$Mg_3(PO_4)_2$. α-Magnesium orthophosphate was prepared by heating 5.055 g (0.012 mole) $Mg_3(PO_4)_2 \cdot 8\,H_2O$ within 5 h to 1173 K and keeping the sample at that temperature for 12 h. A white powder was obtained.

Synthesis of α-$Mg_2P_2O_7$. α-Magnesium diphosphate was prepared by heating 5.1 g (0.029 mole) $MgHPO_4 \cdot 3H_2O$ within 5 h to 1173 K. The final temperature was kept for 4h. After cooling to room temperature a white powder was obtained. The ^{31}P NMR

spectrum showed impurities at -0.2 and -18.8 ppm which are assigned to α-$Mg_3(PO_4)_2$ and the high-temperature phase β-$Mg_2P_2O_7$, respectively. A weak signal is also present at 2.1 ppm which belongs probably to an orthophosphate.

Synthesis of $Mg_2P_4O_{12}$. Magnesium cyclotetraphosphate was prepared by heating a mixture of 1.761 g (0.013 mole) $(NH_4)_2HPO_4$ and 2.324 g (0.013 mole) $MgHPO_4 \cdot 3H_2O$ were ground to a fine powder. The mixture was heated within 20 h to 1273 K and kept at this temperature for 5 h. A white, partly agglomerated powder was obtained after cooling.

Small impurities of magnesium diphosphate were found in the product, which appeared as signals at -13.6 and -19.7 ppm (α-$Mg_2P_2O_7$) as well as -18.7 ppm (β-$Mg_2P_2O_7$) in the ^{31}P NMR spectrum. The impurity phases were also confirmed by reflexes in the diffractogram. $Mg_2P_2O_7$ is build as side product during synthesis of $Mg_2P_4O_{12}$ via

$$2\ MgHPO_4 \rightarrow Mg_2P_2O_7 + H_2O. \tag{25}$$

Integration of the ^{31}P NMR signals in the quantitative spectrum at 25 kHz gives an estimate of less than 3 mole-% phosphorus in the impurity phases.

Synthesis of MgP_4O_{11}. Magnesium ultraphosphate was prepared according to

$$4\ MgHPO_4 \cdot 3\,H_2O + 3\ P_4O_{10} \xrightarrow{600^\circ C} 4\ MgP_4O_{11} + 14\ H_2O\uparrow \tag{26}$$

A mixture of 1.1024 g (0.0063 mole) $MgHPO_4 \cdot 3H_2O$ and 5.9831 g (0.0211 mole) P_4O_{10} was put in a Au-Pd crucible. The sample was heated for 7 d at 873 K. After cooling the excess of P_4O_{10} was removed by boiling the sample for 1 h in a beaker with 100 ml water, filtering and washing the filtrate with ethanol. Small plates of white, slightly grayish color remained which were dried in vacuum.

X-ray diffraction. Powder diffractograms were recorded on a STOE Stadi P powder diffractometer (Cu-$K_{\alpha 1}$, λ=154.05 pm). All synthesized compounds and impurity phases were identified with diffraction patterns in the Stoe WINPOW data base[118].

NMR. ^{31}P MAS NMR spectra were recorded either on a Bruker Avance II 200 spectrometer with a 4.7 T magnet and a commercial MAS probe for 2.5 mm rotors or on a Bruker Avance 500 DSX spectrometer (11.75 T magnet) with commercial MAS probes for 2.5 or 4 mm rotors. ZrO_2 rotors were used. Chemical shifts are given relative to the reference compound 85% H_3PO_4 (T=298 K) as an external standard. Calibration of the spectrometers was done with tetramethylsilane (TMS) under MAS conditions using the unified scale and the chemical shift definitions in[104]. Typically, spectra were recorded by direct excitation with 90° pulses of a few μs length. Various number of scans (up to 600) and repetition delays (up to 1024s) were used to obtain a satisfactory

signal/noise ratio. Isotropic chemical shifts $\delta_{iso} = (\delta_{11} + \delta_{22} + \delta_{33})/3$ were taken directly from NMR spectra at high MAS frequencies ν_{MAS}, typically 25 kHz. Chemical shift anisotropy (CSA) parameters were determined from slowly rotated MAS spectra with the procedure described in [2], where powder spectra simulated with the SIMPSON program[119] are fitted to experimental ones. Dipolar interactions between the nuclear spins were neglected in all simulations. Simulation of a four-spin system including direct dipolar interactions between the four nearest distant ^{31}P nuclei (distances from crystal structure) showed that this approximation is valid even for the very slow MAS spectrum of α-$Mg_3(PO_4)_2$.

CSA results are given according to the *Haeberlen-Mehring-Spiess* convention[120], i.e. in terms of the reduced anisotropy $\delta_{aniso} = \delta_{cc}^{PAF} - \delta_{iso}$ and the asymmetry $\eta = (\delta_{bb}^{PAF} - \delta_{aa}^{PAF})/\delta_{aniso}$, where the shift tensor principal axes eigenvalues δ_{11}^{PAF}, δ_{22}^{PAF}, δ_{33}^{PAF} have been sorted according to $|\delta_{cc}^{PAF} - \delta_{iso}| \geq |\delta_{aa}^{PAF} - \delta_{iso}| \geq |\delta_{bb}^{PAF} - \delta_{iso}|$. The rms deviation of the values is estimated to ±0.1 ppm for δ_{iso}, ±4 ppm for δ_{aniso}, and ±0.04 for η.

6 Results

In the following subsections we apply the EEIM to the calculation of ^{31}P shielding tensors in the crystalline compounds $Mg_2P_4O_{12}$, α-$Mg_3(PO_4)_2$, α-$Mg_2P_2O_7$, and MgP_4O_{11}, whose crystal structures have been described in[107–110]. Structure data and atomic site labelling was taken from the ICSD data base[103], entries 4280, 31005, 15326, 300214, respectively. The atomic labels are used in the subsequent presentation of the results. For ease and in order to avoid ambiguities we show the unit cells in the supplemental material.

All compounds were resynthesized and the powdered samples were characterized by their X-ray diffraction pattern as well as ^{31}P MAS NMR spectrocopy. Experimental ^{31}P chemical shift tensor eigenvalues were obtained from slowly rotated MAS spectra. In spite of the similarity in their chemical composition, the four phosphates are quite different with respect to the chaining pattern of PO_4 tetrahedra which allows us to demonstrate the different strategies for the cluster construction. According to the Q_n nomenclature introduced in[121] (n gives the number of bridging oxygen atoms of a PO_4 tetrahedron to neighboring tetrahedrons) the compounds in the order above are composed of Q_2, Q_0, Q_1, and infinitely chained Q_2/Q_3 units. The different Q_n groups can be easily distinguished by means of their significantly different ^{31}P chemical shift and CSA parameters[122]. All crystals except for α-$Mg_3(PO_4)_2$ possess more than one P-site of the same Q_n type, whose isotropic chemical shifts are only slightly different. The EEIM calculations allow the assignment of the NMR signals to the sites.

6.1 Magnetic shielding tensor in $Mg_2P_4O_{12}$

The crystal structure[107] of magnesium cyclotetraphosphate, $Mg_2P_4O_{12}$, contains C_i symmetric tetraphosphate rings, $[P_4O_{12}]^{4-}$, in half-chair conformation which contain two times the two independent crystallographic P sites (P1,P2) and the six independent O sites (O1–O6). Each P- and O-site occurs eight times in the unit cell. Two independent Mg sites are present (Mg1,Mg2), each occurring four times in the unit cell.

The NMR spectrum is shown in Fig. 8. Two signals P_A and P_B are observed at δ=-34.6 ppm and δ=-36.8 ppm, respectively, which agree with the rough values given in[123]. Experimental CSA parameters of P_A and P_B are collected together with calculated ones in Tab. 1.

Various quantum clusters (QCs) shown in Fig. 7 are used for EIM, EEIM and non-embedded cluster calculations. Details of the cluster setup and figures of two additional clusters – $[Mg_2P_4O_{12}]^0_7$ and $[Mg_2P_4O_{12}]^0_{13}$ – used to demonstrate the convergence of the QC expansion are given in the supplemental material. All QCs are C_i symmetric so that artificial dipole moments are avoided. A locally dense basis is used where the central P_4O_{12}-ring is described with 6-311G(3df,3pd) bases or better and the farther distant atoms are described with 6-31G(d,p) bases or even a minimal CEP-4G valence bases with pseudopotentials for the core electrons. The QC $[P_4O_{12}]^{4-}$ (Fig. 7a) is the usual choice for the traditional EIM procedure. As it does not contain Mg sites, the embedding charges corresponding to Mg have to be fixed to +2 in order to ensure charge neutrality of the unit cell. The second QC $[Mg_2P_4O_{12}]^0$ (Fig. 7b) contains one formula unit of the compound. It does not contain the atomic site Mg2, however, and therefore we use the *atomic grouping* Mg={Mg1,Mg2} so that q(Mg2)= q(Mg1) is enforced for the Ewald summation. The correct 1:1 ratio of crystallographic Mg1, Mg2 sites is also not present in QCs $[Mg_2P_4O_{12}]^0_3$ (Fig. 7c, Mg1:Mg2=2:4), $[Mg_2P_4O_{12}]^0_5$ (Fig. 7d , Mg1:Mg2=6:4), $[Mg_2P_4O_{12}]^0_7$ (Mg1:Mg2=8:6), and $[Mg_2P_4O_{12}]^0_{13}$ (Mg1:Mg2=12:14), all of which have been calculated with the same atomic grouping. While Mg1 and Mg2 sites (Wyckoff symbols 4*e* and 4*d*, repectively) occur in the UC only with half frequency relative to the other atomic sites (Wyckoff symbol 8*f*), the grouped type Mg occurs with the same relative frequency of eight. The clusters were constructed in a semiautomatic manner, e.g. $[Mg_2P_4O_{12}]^0_{13}$ was created by filling spheres with a radius $r_P = 5$ Å around the four P-atoms of the central P_4O_{12} ring. Then, the covalent fragments were completed and a proper amount of Mg atoms was added in order to make the QC neutral.

The EEIM results are superior to EIM. The results of the different cluster calculations are compared in more detail in section 6.5. Here, we focus on the chemical shift tensor eigenvalues calculated with the QC $[Mg_2P_4O_{12}]^0_5$ which are given in Tab. 1 and which suggest the following assignment between experimental NMR signals and crystallographic sites: P_A belongs to P1, and P_B belongs to P2. This results in a root mean square deviation of $RMSD(\delta^{exp}_{iso}, \delta^{calc}_{iso}) = 1.1$ ppm between experimental and calculated isotropic chemical shifts and $RMSD(\delta^{exp}_{ii}, \delta^{calc}_{ii}) = 5.9$ ppm between

the principal axis values. The reverse assignment would result in bigger deviations ($RMSD(\delta_{iso}^{exp}, \delta_{iso}^{calc}) = 2.2\,\text{ppm}$, $RMSD(\delta_{ii}^{exp}, \delta_{ii}^{calc}) = 8.4\,\text{ppm}$). Further confidence for the assignment $P_A \leftrightarrow$ P1, $P_B \leftrightarrow$ P2 comes from the fact that any other of the embedded calculations lead to the same result.

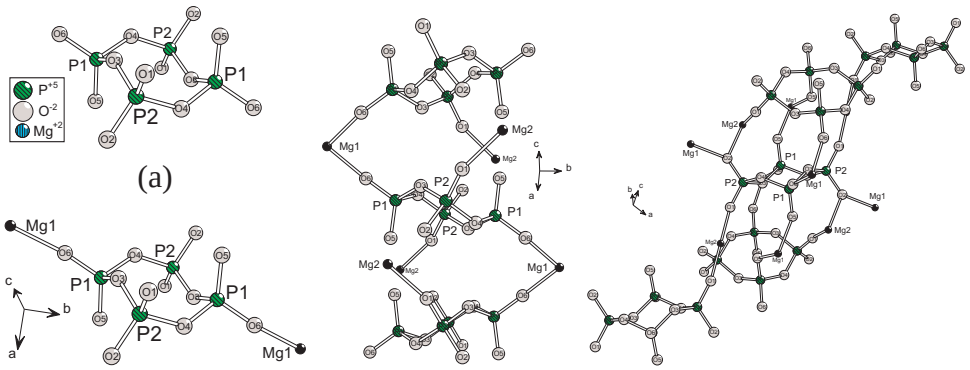

Figure 7: Various $Mg_2P_4O_{12}$ clusters. (a): $[P_4O_{12}]^{4-}$, (b): $[Mg_2P_4O_{12}]_1^0$, (c): $[Mg_2P_4O_{12}]_3^0$, (d): $[Mg_2P_4O_{12}]_5^0$. Central P atoms with off-centered labels denote reference points for the local expansion.

Table 1: Calculated and experimental ^{31}P chemical shift parameters of various magnesium phosphates. Pairs of subsequent lines give the assignment of crystallographic sites to NMR signals. Calculated values use the site labelling of the crystal structures referenced in the text, experimental signals are labelled in Fig. 8. For convenience CSA the principal axes values are given in col. 6-8.

Calc. No	site/ signal	δ_{iso} [a] / ppm	δ_{aniso} [a] / ppm	η	δ_{11} [a] / ppm	δ_{22} [a] / ppm	δ_{33} [a] / ppm
magnesium cyclotetraphosphate, $Mg_2P_4O_{12}$							
calc.[b]	P1	-33.8	-118	0.469	53.1	-2.3	-152.1
exp.	P_A	-34.6	-124	0.459	55.9	-1.0	-158.6
calc.[b]	P2	-35.5	-127	0.401	53.0	2.4	-162.1
exp.	P_B	-36.8	-134	0.475	61.7	-1.7	-170.4
magnesium orthophosphate, α-$Mg_3(PO_4)_2$							
calc.[b]	P1	-5.8	-9	0.787	2.5	-4.8	-15.1
exp.	P	-0.1	-16	0.640	12.7	2.7	-15.8
magnesium diphosphate, α-$Mg_2P_2O_7$							
calc.[b]	P1	-23.4	78	0.408	54.7	-46.5	-78.4
exp.	P_B	-19.7	85	0.321	65.4	-48.6	-75.9
(exp.[c]	P_B	-20.2	84	0.3	63.8	-49.6	-74.8)
calc.[b]	P2	-14.3	58	0.052	43.7	-41.8	-44.9
exp.	P_A	-13.4	68	0.162	54.7	-42.0	-53.0
(exp.[c]	P_A	-13.8	71	0.1	57.2	-45.8	-52.9)
magnesium ultraphosphate, MgP_4O_{11}							
calc.[b]	P1	-39.2	-163	0.312	68.0	16.9	-202.5
exp.	P_A	-38.4	-174	0.361	80.3	17.4	-212.8
(exp.[d]	P_A	-38.7	-174	0.33	77.0	19.6	-212.7)
calc.[b]	P2	-44.0	-132	0.172	33.4	10.7	-176.2
exp.	P_C	-45.5	-147	0.183	41.6	14.6	-192.7
(exp.[d]	P_C	-46.1	-150	0	28.9	28.9	-196.1)
calc.[b]	P3	-51.6	-128	0.130	20.8	4.2	-179.7
exp.	P_D	-51.2	-141	0.219	34.5	3.8	-192.0
(exp.[d]	P_D	-51.7	-144	0	20.3	20.3	-195.7)
calc.[b]	P4	-43.1	-155	0.354	62.0	7.0	-198.4
exp.	P_B	-43.3	-171	0.396	76.1	8.3	-214.4
(exp.[d]	P_B	-43.7	-174	0.33	72.0	14.6	-217.7)

[a] chemical shifts calculated from absolute magnetic shieldings according to eq. 24.
[b] only calculated values for the central P-atom(s) are given (labelled in figures), even if more P-atoms are present in the cluster
[c] literature data from [124]. Other data for P_A are: δ_{iso}=-14.0 ppm from [125] or δ_{iso}=-14.7 ppm from [126]; other data for P_B are: δ_{iso}=-20.3 ppm from [125], -20.0 ppm from [126].
[d] literature data from [125]

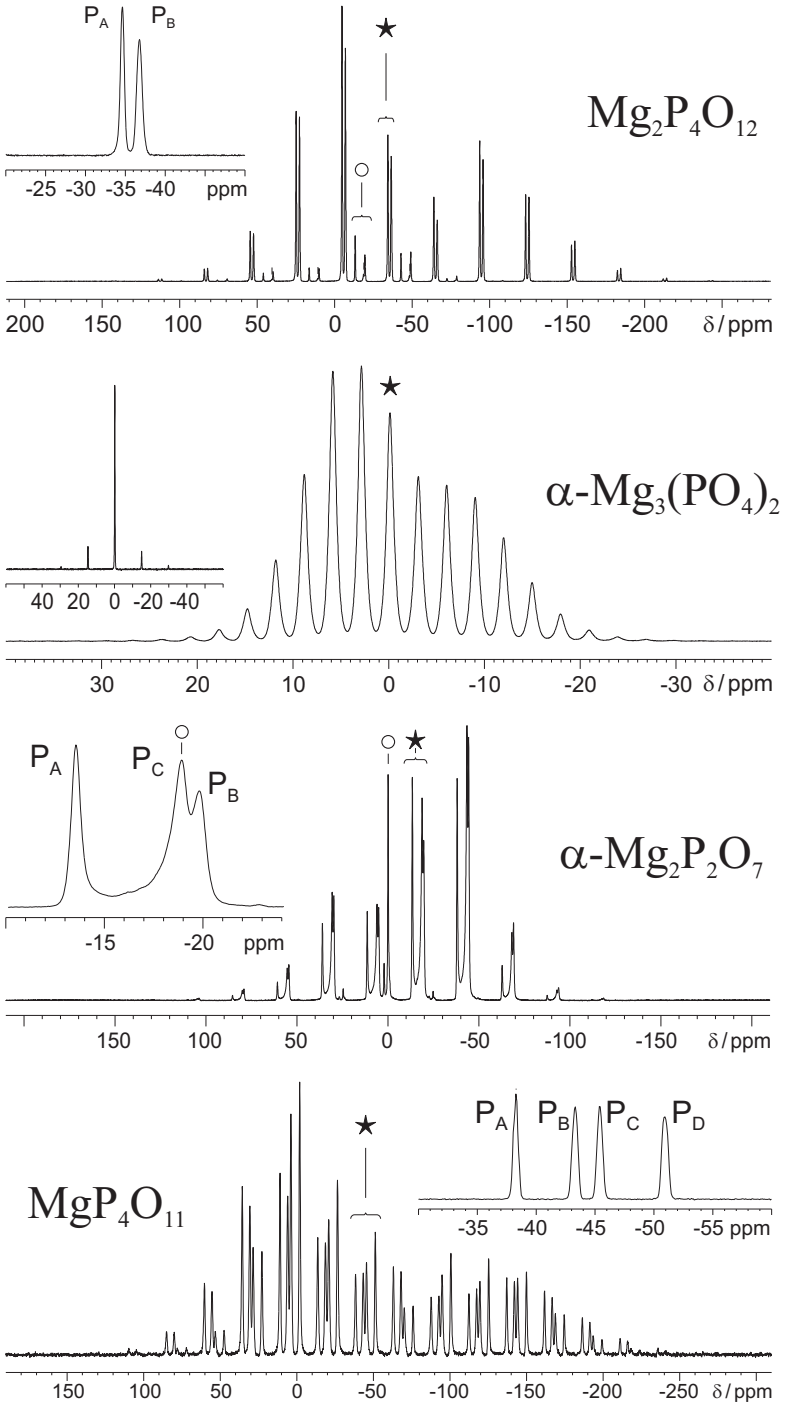

Figure 8: Solid state ^{31}P-MAS-NMR spectra of magnesium phosphates. Regions of the isotropic bands are highlighted by a star (⋆) and are enlarged in an inset. Sample impurities denoted by a circle (○) are discussed in section 5. From top to bottom: $Mg_2P_4O_{12}$ (ν_{MAS}=6 kHz, B_0=11.75 T, inset: 25 kHz, B_0=4.7 T), α-$Mg_3(PO_4)_2$ (ν_{MAS}=600 Hz, B_0=11.75 T, inset: ν_{MAS}=3 kHz), α-$Mg_2P_2O_7$ (ν_{MAS}=5 kHz, B_0=11.75 T), MgP_4O_{11} (ν_{MAS}=2 kHz, B_0=4.7 T, inset: ν_{MAS}=25 kHz).

6.2 Magnetic shielding tensor in α-$Mg_3(PO_4)_2$

The unit cell of α-magnesium phosphate, α-$Mg_3(PO_4)_2$, contains the seven sites Mg1, Mg2, P1, O1, O2, O3, O4 with the frequencies 4, 2, 4, 4, 4, 4, 4, respectively[108]. The crystal is composed of $[PO_4]^{3-}$ anions (Q_0-phosphate) surrounded by seven Mg^{2+} cations in the next coordination sphere.

The ^{31}P MAS NMR spectrum at 3 kHz shows the center signal at δ=-0.1 ppm. CSA parameters are obtained from the MAS-NMR spectrum shown in Fig. 8, where the MAS frequency was reduced to 600 Hz in order to obtain a sufficient number of rotational side bands necessary for a reliable determination of such small anisotropies. Experimental CSA values are given together with calculated ones in Tab. 1.

Quantum clusters shown in Fig. 9 are used for non-embedded and (E)EIM calculations. Details of the cluster setup are given in the supplemental material. The charged phosphate unit $[PO_4]^{3-}$ (Fig. 9a) displays the usual choice for an EIM procedure. Atomic charges are redistributed on the P and the O sites, whereas the charges on Mg have to be fixed to the formal charge +2 (enforced by QC charge definition and UC electroneutrality). The QCs $[Mg_3(PO_4)_2]_1^0$ (Fig. 9b), $[Mg_3(PO_4)_2]_5^0$ (Fig. 9c), and $[Mg_3(PO_4)_2]_8^0$ (Fig. 9d) are designed according to EEIM recommendations, i.e. they are electroneutral and contain the atomic sites with the same relative frequency as the UC. Among the non-embedded calculations only QC $[PO_4]^{4-}$ shows accidentally a reasonable result ($RMSD(\delta_{ii}^{exp}, \delta_{ii}^{calc})$=6.0 ppm), whereas the remaining ones display unrealistic NMR parameters ($RMSD(\delta_{ii}^{exp}, \delta_{ii}^{calc})$=40.6, 24.0 ppm for $[Mg_3(PO_4)_2]_1^0$ and $[Mg_3(PO_4)_2]_5^0$, respectively) or convergence problems ($[Mg_3(PO_4)_2]_8^0$).

EIM and EEIM calculations lead to comparable results. The EIM calculation yields $RMSD(\delta_{ii}^{exp}, \delta_{ii}^{calc})$=7.7 ppm. The smallest possible neutral QC, $[Mg_3(PO_4)_2]^0$, gives the best result ($RMSD(\delta_{ii}^{exp}, \delta_{ii}^{calc})$=6.5 ppm), although the nearest coordination sphere around the central phosphate ion is only partially filled. An acceptable result is also obtained with the QC $[Mg_3(PO_4)_2]_5^0$ with $RMSD(\delta_{ii}^{exp}, \delta_{ii}^{calc})$=7.4 ppm. Corresponding shift parameters are collected in Tab. 1. The result from QC $[Mg_3(PO_4)_2]_8^0$ is slightly worse ($RMSD(\delta_{ii}^{exp}, \delta_{ii}^{calc})$=7.7 ppm).

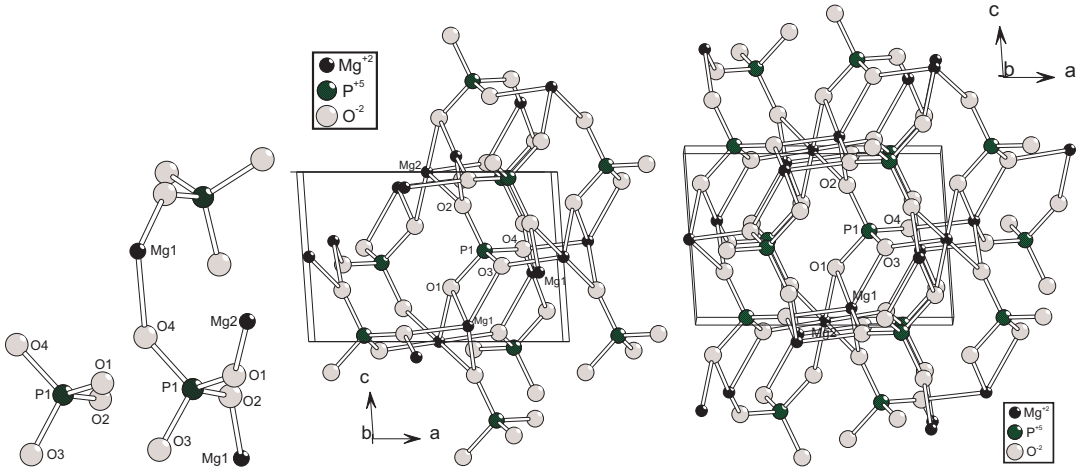

Figure 9: Clusters chosen for EEIM calculations on α-$Mg_3(PO_4)_2$. (a): $[PO_4]^{3-}$ (b): $[Mg_3(PO_4)_2]^0$, (c): $[Mg_3(PO_4)_2]^0_5$. (d): $[Mg_3(PO_4)_2]^0_8$. The central phosphate unit is highlighted with atomic site labels from the crystal structure.

6.3 Magnetic shielding tensor in α-$Mg_2P_2O_7$

Crystal structures of α-magnesium diphosphate, α-$Mg_2P_2O_7$, have been reported by Calvo[109] and Łukaszewicz[127]. In this work the probably more reliable structure of Calvo is preferred as well as the site labelling given there. The unit cell of α-$Mg_2P_2O_7$ contains eight formula units with two independent P-sites (P1,P2), seven O-sites (O1–O7) and two Mg-sites (Mg1,Mg2). Of the two P atoms in a diphosphate anion $[P_2O_7]^{4-}$ (Q_1 phosphate) the P2 atom has the shorter distance to the bridging oxygen.

The ^{31}P MAS NMR spectrum shows two isotropic signals at -13.4 (signal P_A) and -19.7 ppm (P_B). Experimental ^{31}P CSA parameters were determined from the slow-MAS NMR spectrum in Fig. 8 and are collected in Tab. 1. The CSA values are in fair agreement with earlier determinations[124–126,128], except for the most recent, but probably wrong, work of Moreno *et al.*[129] where only a single ^{31}P signal with δ_{iso}=-5.9 ppm (δ_{11}=74 ppm, δ_{22}=-21 ppm, δ_{33}=-71 ppm) is mentioned. This signal could belong to one of two P-sites in the hydrate $Mg_2P_2O_7 \cdot 3.5\,H_2O$ whose chemical shift was reported at -5.44 ppm in[130]. Our sample shows a significant fraction of the high-temperature phase β-$Mg_2P_2O_7$[131,132] (signal P_C at 18.8 ppm) that was included in the fit procedure.

Non-embedded, EIM and EEIM calculations were performed using the quantum clusters shown in Fig. 10. The $[P_2O_7]^{4-}$ cluster is the common choice for traditional EIM calculations. The uncharged QC $[Mg_2P_2O_7]^0_9$ was constructed in an semiautomatic manner according to EEIM recommendations: First, a $[P_2O_7]^{4-}$ ion was selected. Second, the ion was augmented with sites that fall in spheres with a radius of 5 Å around the two P-nuclei. Third, anionic fragments were completed and electroneu-

trality was achieved by adding the proper amount of Mg counter ions. No symmetry was used in the construction of the QC. Details of the QC setup are given in the supplemental material.

The ^{31}P NMR chemical shifts calculated with the EEIM show the best agreement with the experimental results and are given in Tab. 1. Values of the EIM calculation are significantly too shielded ($\delta_{iso}(P1)$ =-28.4 ppm, $\delta_{iso}(P2)$ =-16.4 ppm), probably due to the charge mismatch in $[P_2O_7]^{4-}$. The non-embedded calculations show a worse agreement or convergence problems. The assignment of NMR signal P_A to the crystallographic site P2 and signal P_B to site P1 is unambigous, since $RMSD(\delta_{ii}^{exp}, \delta_{ii}^{calc})$=7.2 ppm whereas the inverse assignment would have $RMSD(\delta_{ii}^{exp}, \delta_{ii}^{calc})$=18.9 ppm. All other calculations based on Calvos structure lead to the same assignment. Moreover, the assignment $P_A \leftrightarrow$P2, $P_B \leftrightarrow$P1 is also obtained from EEIM calculations based on the crystal structure of Łukaszewicz, but the deviation between experimental and calculated shift tensor eigenvalues is larger ($RMSD(\delta_{ii}^{exp}, \delta_{ii}^{calc})$=7.9 ppm).

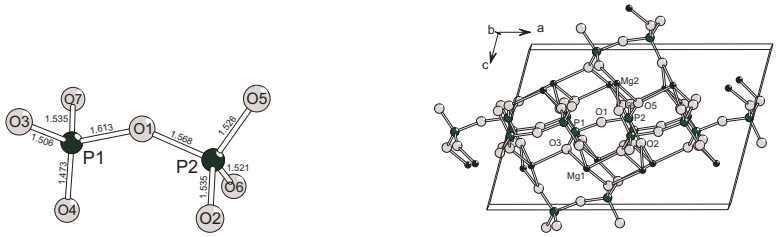

(a) (b)

Figure 10: Quantum clusters of α-$Mg_2P_2O_7$ used in (E)EIM calculations. (a): $[P_2O_7]^{4-}$, (b): $[Mg_2P_2O_7]_9^0$. P atoms with off-centerd labels denote reference points for the local expansion.

6.4 Magnetic shielding tensor in MgP_4O_{11}

The unit cell of magnesium ultraphosphate, MgP_4O_{11}, contains $Z = 4$ formula units, one magnesium site (Mg1), eleven oxygen sites (O1–O11), and four phosphorus sites (P1–P4)[110]. The crystallographic sites P2 and P3 are Q_3 phosphates, whereas the sites P1 and P4 are Q_2 phosphates.

The ^{31}P MAS NMR spectrum in Fig. 8 shows four central peaks at P_A=-38.4 ppm, P_B=-43.3 ppm, P_C=-45.5 ppm and P_D=-51.2 ppm, which is in fair agreement with previous data of Feike *et al.*[125]. Experimental ^{31}P CSA parameters were determined from the slow-MAS spectrum and are given in Tab. 1.

Since the phosphate tetrahedra in MgP_4O_{11} form an infinite polymeric network, it is impossible to select a covalently saturated, formally charged ion as required by the conventional EIM approach. In contrast, the EEIM guidelines allow to choose various clusters. As the distance between the four different P sites in the unit cell is rather big for building a single cluster containing all sites, we split the problem into two separate

calculations. With the first QC of the sum formula $[MgP_4O_{11}]_6^0$ (see Fig. 11a) we focus on the NMR parameters for P1 and P2 sites. Values of P3 and P4 sites are not expected to be reliable in these calculations as the sites are described only with a 6-31G(d,p) basis and are located near the cluster boundary where dangling bonds are present. The second QC, $[MgP_4O_{11}]_5^0$ (Fig. 11b), is constructed to obtain reliable NMR parameters for P3 and P4, whereas parameters for the P1 and P2 sites are unreliable. Details of the cluster setup are given in the supplemental material.

The non-embedded calculation on $[MgP_4O_{11}]_6^0$ showed no convergence, so that a complete set of ^{31}P NMR parameters for MgP_4O_{11} could only be obtained from EEIM calculations. The results are collected in Tab. 1 and allow a complete assignment of experimental NMR signals to crystallographic sites:† The calculated order of isotropic chemical shifts suggests that resonance P_A corresponds to site P1, P_B to site P4, P_C to P2 and P_D to P3 ($RMSD(\delta_{iso}^{exp}, \delta_{iso}^{calc})$=0.9 ppm). Any other assignment would result in a bigger $RMSD(\delta_{iso}^{exp}, \delta_{iso}^{calc})$. Comparison of experimental and calculated CSA parameters supports our assignment ($RMSD(\delta_{ii}^{exp}, \delta_{ii}^{calc})$=10.8 ppm). Again, any other assignment would lead to a bigger $RMSD(\delta_{ii}^{exp}, \delta_{ii}^{calc})$. Further confirmation comes from the ^{31}P 2D double quantum spectrum in[125], which shows a connectivity chain P_A-P_C-P_D-P_B. According to our assignment this corresponds to the site chain pattern P1-P2-P3-P4, which is indeed found in the crystal structure.

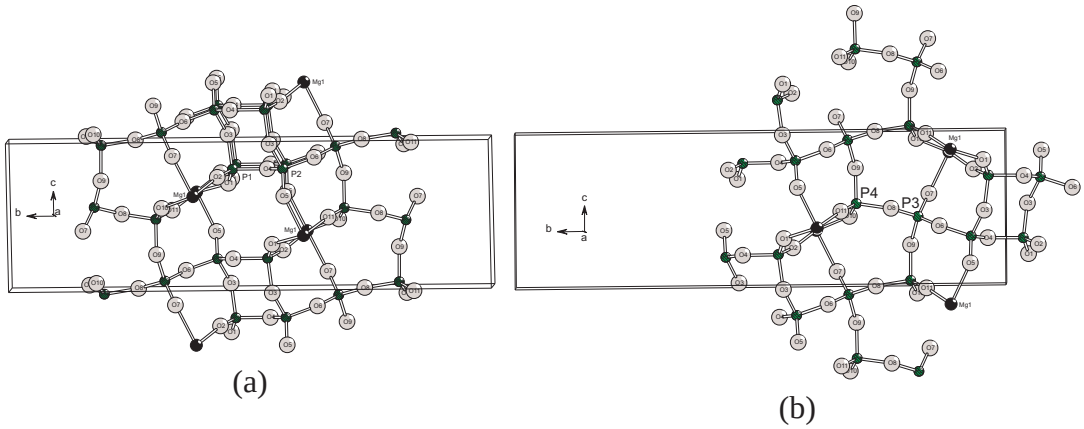

(a) (b)

Figure 11: Quantum clusters for the calculation of NMR parameters in magnesium ultraphosphate. (a): $[MgP_4O_{11}]_6^0$ cluster for calculation of P1 and P2 sites, (b): $[MgP_4O_{11}]_5^0$ cluster for calculation of P3 and P4 sites. Phosphorus sites with off-centered labels denote reference points for the locally dense basis expansion.

† A partial assignment was already presented in the work of Feike *et al.*, where – on the basis of CSA parameters – P_A and P_B were related to Q_2 sites and P_C and P_D to Q_3 sites.

6.5 Comparison of non-embedded, EIM and EEIM calculations

A more accurate description of NMR parameters is expected from EEIM calculations in comparison to traditional EIM calculations, because the charge misfit is avoided and the quantum mechanically treated region is usually enlarged. Within the EEIM framework there is always freedom in choosing a bigger QC, but the question is if the increased QC size pays off. Larger QCs are also commonly used in non-embedded calculations in order to account for the most prominent long-range terms[7,133]. In the limit of infinitely large QCs EEIM and non-embedded calculations give the same result. It is therefore interesting to investigate the convergence of the NMR parameters with respect to the QC size for EEIM and non-embedded calculations.†

For this purpose we expanded the series of QCs for $Mg_2P_4O_{12}$ (section 6.1, Fig. 7) with two further elements, $[Mg_2P_4O_{12}]^0_7$ and $[Mg_2P_4O_{12}]^0_{13}$. Figures and details of the cluster setup are described in the supplemental material. Fig. 12 shows the dependence of the root mean square deviation $RMSD(\delta_{ii}^{exp}, \delta_{ii}^{calc})$ of chemical shift tensor eigenvalues with respect to the QC size. In case of non-embedded cluster calculations widely varying values occur for different QC sizes, which indicates that convergence is difficult to achieve in such an approach. The $RMSD(\delta_{ii}^{exp}, \delta_{ii}^{calc})$ is significantly higher than in EEIM calculations. The failed convergence with QC $[Mg_2P_4O_{12}]^0_{13}$ displays another problem of non-embedded calculations.

The situation is much more satisfacory for embedded calculations, where the variation in eigenvalues for different QC choices is considerably smaller. The traditional EIM calculation gives already a reasonable result ($RMSD(\delta_{ii}^{exp}, \delta_{ii}^{calc})$=11.4 ppm) that allows the signal assignment. Further improvement is achieved in the series of EEIM calculations using $[Mg_2P_4O_{12}]^0_1$, $[Mg_2P_4O_{12}]^0_3$, and $[Mg_2P_4O_{12}]^0_5$ where $RMSD(\delta_{ii}^{exp}, \delta_{ii}^{calc})$ decreases monotonically from 10.0 ppm, over 6.7 ppm to 5.9 ppm. Calculations with larger QCs show no improvement over $[Mg_2P_4O_{12}]^0_5$ and indicate that the QC size is not the main source of error any more. The reason for the slight worsening of $RMSD(\delta_{ii}^{exp}, \delta_{ii}^{calc})$ in $[Mg_2P_4O_{12}]^0_7$ (6.9 ppm) and $[Mg_2P_4O_{12}]^0_{13}$ (9.0 ppm) is unclear so far. It might be related to the locally dense basis where an increased number of pseudopotentials is employed at farther distances from the reference points. The neglect of core contributions to the magnetic shielding and the wrong nodal structure of the wave function at the remote centers might introduce a small but systematic error in the calculation of the magnetic shielding at the reference point. Another reason might be polarization effects at the QC boundary.

Convergence with respect to the atomic basis expansion at the nuclei of interest was investigated for $[Mg_2P_4O_{12}]^0_5$. Three radial shells were used in the default setup where a 6-311G(3df,3pd) basis was used in the range $r_1 \in [0, 2.5[$ Å, a 6-31G(d,p) basis in the range $r_2 \in [2.5, 5[$ Å, and a CEP-4G basis and PPs in the range $r_3 \geq 5$Å, supple-

† In this section we omit a comparison of the EEIM with the EIM/cluster approach because, to the best of our knowledge, a detailed strategy for cluster construction is absent in EIM/cluster, which may lead to ambiguous results. Moreover, the calculation of large EIM clusters would be extremely expensive without a locally dense basis.

mented with *d* functions on P atoms in the range between 5.0 and 6.9 Å. Very similar results are obtained, when the 6-311G(3df,3dp) set in range r_1, i.e. at the atoms of the central P_4O_{12}-ring, is augmented by diffuse functions to give the 6-311++G(3df,3dp) set. The biggest deviation in a shielding tensor eigenvalue between the two calculations amounts to 0.9 ppm and the eigenvector orientations are identical within 0.2°. This indicates that diffuse basis functions are not required for a proper calculation of NMR parameters in solids. Deviations of δ_{ii}^{calc} with respect to the experimental results turn out to be insignificantly smaller in the 6-311++G(3df,3dp) calculation ($RMSD(\delta_{ii}^{exp}, \delta_{ii}^{calc})$ =5.7 ppm), provided the specific parameters *A* and *B* for the 6-311++G(3df,3dp) basis are used in conversion equation 24. Reducing the basis at the atoms of the central P_4O_{12}-ring to 6-31G(d,p) quality leads to maximum deviation of 88.4 ppm in shielding tensor eigenvalues and to 1.4° in the eigenvector orientations. The big change in σ_{ii}^{calc} is in parts a systematic basis set specific deviation, but considering the significant increase of $RMSD(\delta_{ii}^{exp}, \delta_{ii}^{calc})$ =11.4 ppm (δ_{ii}^{calc} calculated with the 6-31G(d,p) basis set specific parameters in conversion equation 24) reveals that the double-ζ basis is not flexible enough for the prediction of NMR parameters in a wider range of phosphorus compounds.

A change of basis functions in the outermost radial shell has a minor effect on the calculated shielding tensors. This is demonstrated in a another calculation on $[Mg_2P_4O_{12}]_5^0$ where we replaced the CEP-4G basis in shell range r_3 of the default calculation by a 6-31G(d,p) set. The resulting shielding tensor eigenvalues deviate by less than 3.0 ppm from the default calculation and the eigenvectors coincide within 1.1°. The chemical shift tensor eigenvalues deviate from the experimental ones by $RMSD(\delta_{ii}^{exp}, \delta_{ii}^{calc})$ =6.1 ppm. This indicates that at larger distances from the nuclei of interest (> 5.0Å), pseudopotentials and minimal bases may be employed to save computational resources without a significant loss in accuracy.

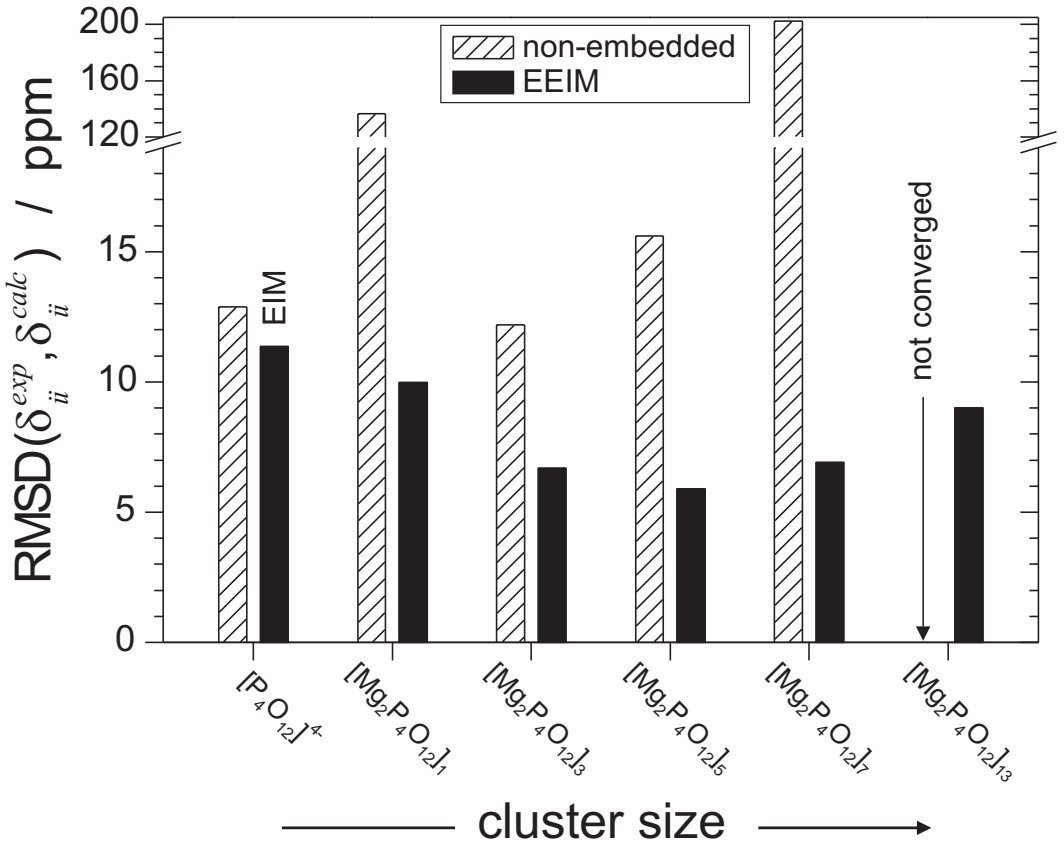

Figure 12: Root mean square deviation of the six ^{31}P chemical shift tensor eigenvalues in $Mg_2P_4O_{12}$ calculated with various cluster models relative to the experimental values.

Similar observations were made for α-$Mg_3(PO_4)_2$, α-$Mg_2P_2O_7$, MgP_4O_{11}. In total, 27 shift tensor eigenvalues were calculated by EEIM (see Tab. 1), 15 by EIM[†] and 21 by non-embedded cluster calculations[‡] which are plotted against the experimental values in Fig. 13. Within the 15 eigenvalues that are available for all three types of cluster calculations, EEIM performs best with $RMSD(\delta_{ii}^{exp}, \delta_{ii}^{calc})$ =6.8 ppm. It improves the $RMSD(\delta_{ii}^{exp}, \delta_{ii}^{calc})$ =10.1 ppm of EIM by about $\frac{1}{3}$. Non-embedded calculations give the worst result with $RMSD(\delta_{ii}^{exp}, \delta_{ii}^{calc})$ =21.2 ppm, although the best available results were chosen when more than one non-embedded cluster calculation converged.

Taking into account all 27 data for EEIM, i.e. including the 12 eigenvalues from the covalently networked MgP_4O_{11}, leads to $RMSD(\delta_{ii}^{exp}, \delta_{ii}^{calc})$ =8.8 ppm, which is still superior to the *RMSD* of EIM. This indicates that networked solids can be treated by

[†] The covalently networked MgP_4O_{11} cannot be calculated by EIM. [‡] For cluster $[MgP_4O_{11}]_6^0$ (Fig. 11a) the non-embedded cluster calculation did not converge.

EEIM without a substantial loss in accuracy[†]. It should be noted that all *RMSD*s given above were obtained with δ_{ii}^{calc} values derived from the general conversion equation (24) that is valid for a larger ^{31}P shift range.

The *RMSD*s are significantly smaller if only the shielding for the magnesium phosphates are taken into account in the fitting procedure[‡], $RMSD(\delta_{ii}^{exp}, \delta_{ii}^{calc})$=4.3 ppm in case of EEIM ($\delta_{ii}^{calc} = \{\sigma_{ii}^{calc} - 307.19\,\text{ppm}\}/-1.0237$, N=27 eigenvalues), $RMSD(\delta_{ii}^{exp}, \delta_{ii}^{calc})$= 4.4 ppm in case of EIM ($\delta_{ii}^{calc} = \{\sigma_{ii}^{calc} - 311.25\,\text{ppm}\}/-0.9905$, N=15) and $RMSD(\delta_{ii}^{exp}, \delta_{ii}^{calc})$= 21.1 ppm in case of non-embedded calculations ($\delta_{ii}^{calc} = \{\sigma_{ii}^{calc} - 309.33\,\text{ppm}\}/-0.9508$, N=21). Fig. 13 shows linear regression curves for the corresponding fits in a plot of δ_{ii}^{calc} versus δ_{ii}^{exp}. Obviously, an error compensation takes place for chemically similar compounds. Such a small *RMSD* which is in the range of the experimental error for δ_{ii}^{exp} is probably not representative for the general accuracy of the EEIM method. But even with the former value of 8.8 ppm the *RMSD* of EEIM values is less than the standard deviation of 9.6 ppm derived for conversion equation (24) where only isotropic shifts are used. This indicates that the shortcomings of the quantum chemical method and the chosen atomic basis are probably more significant than the errors introduced by the embedding scheme.

[†] Although the number of data points is rather small for a reliable statistical estimate, we believe that the decribed trends are correct. Unpublished results on further phosphorus compounds, $K_3(PO_2NH)_3$, $Na_3(PO_2NH)_3{\cdot}H_2O$, $(NH_4)_4(PO_2NH)_4 \cdot 4H_2O$, $Mg_2(PO_2NH)_4 \cdot 8H_2O$, $LaPO_4$, $La(PO_3)_3$, and $LaP_3O_9 \cdot 3H_2O$ extend the data base to 45 shift tensor eigenvalues for EIM and 63 for EEIM. For EIM we obtained $RMSD(\delta_{ii}^{exp}, \delta_{ii}^{calc})$ =9.8 ppm, whereas for EEIM $RMSD(\delta_{ii}^{exp}, \delta_{ii}^{calc})$ =8.3 ppm.

[‡] This type of "internal calibration" has been used in GIPAW calculations on $\beta-$ and $\gamma-Ca(PO_3)_2$ in [16]. For the 24 eigenvalues presented in Table 1 of that work we calculate $RMSD(\delta_{ii}^{exp}, \delta_{ii}^{calc})$=8.4 ppm.

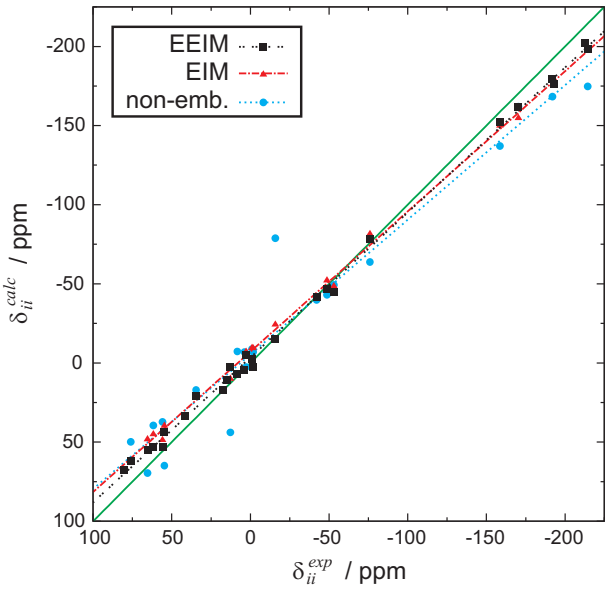

Figure 13: Correlation plot of experimental ^{31}P shift tensor eigenvalues versus calculated eigenvalues by EEIM (■), EIM (▲), and non-embedded (●) cluster methods (δ_{ii}^{calc} obtained via eq. 24). The solid diagonal line (green in color plot) indicates the ideal correlation. The other lines are regression curves from internal calibrations to EEIM (black, N=27), EIM (red, N=15) and non-embedded (cyan, N=21) data sets when only magnesium phosphates are used. N gives the number of sample points.

In general, isotropic chemical shifts are calculated more accurately than shift tensor eigenvalues. This comes in part from a statistical error compensation. The error $\Delta\delta_{iso}^{calc}$ in calculated isotropic chemical shifts and the error $\Delta\delta_{ii}^{calc}$ of calculated shift tensor eigenvalues are related by the equation $\delta_{iso} = \frac{1}{3}\sum_i \delta_{ii}$, $(i = 1, 2, 3)$. If $\Delta\delta_{ii}^{calc}$ is assumed to be identical for all i one obtains by error propagation

$$\Delta\delta_{iso} = \frac{1}{\sqrt{3}}\Delta\delta_{ii} \quad . \tag{27}$$

Another reason for the reduced $\Delta\delta_{iso}^{calc}$ is that errors in the angular electron density distribution around a nucleus lead to a systematic distortion of the shielding tensor with one eigenvalue increased and another one reduced. We obtain $RMSD(\delta_{iso}^{exp}, \delta_{iso}^{calc})$=2.4, 5.4, and 3.8 ppm for EEIM, EIM and non-embedded methods, respectively, when δ_{iso}^{calc} is calculated from σ_{iso}^{calc} by the general conversion equation. Using the above mentioned conversion equations, that are restricted to magnesium phosphates, the values reduce to $RMSD(\delta_{iso}^{exp}, \delta_{iso}^{calc})$=1.6, 2.8, and 6.4 ppm, respectively.

7 Conclusion

A new implementation of the *Embedded Ion Method* (EIM) and the EIM/cluster approach was presented, useful for the calculation of NMR parameters of crystalline compounds. Shortcomings and ambiguities of the traditional methods were discussed. An improved scheme named EEIM was suggested, that avoids or reduces the problems by setting up guidelines for the quantum cluster (QC) construction. Basic advantages of the new scheme are the self-consistency of all embedding charges and the independence of empirical parameters such as formal charges. In this sense the scheme is self-contained. Uncharged QCs are recommended, which can be obtained by using the same relative site frequencies in the QC as in the unit cell. Alternatives, like *atomic grouping*, are discussed for cases where exact charge neutrality is not possible. In any case the nuclei of interest should be located near the center of the QC with a buffer zone of at least two to three coordination spheres to the QC boundary. The boundary should be drawn between atoms with ionic interactions. Covalently networked crystals can be treated, too, if the dangling bonds are far enough from the nuclei of interest. A locally dense atomic orbital basis is employed to calculate larger QCs at reduced computational costs. A semiautomatized cluster setup is presented, which is more efficient and less error-prone than a manual setup.

The accuracy of NMR parameters from EEIM calculations was sufficient to allow the new assignment of various experimental ^{31}P NMR signals to crystallographic sites in the magnesium phosphates $Mg_2P_4O_{12}$, α-$Mg_3(PO_4)_2$, α-$Mg_2P_2O_7$ and MgP_4O_{11}. The inner shell region of all QCs were treated at mPW1PW/6-311G(3df,3pd) level. 27 chemical shift tensor eigenvalues were calculated with a root mean square deviation (*RMSD*) of 8.8 ppm relative to experimental values when a general conversion equation from ^{31}P absolute magnetic shieldings to chemical shifts was used. A conversion equation derived specifically for the magnesium phosphates led to a *RMSD* of 4.3 ppm. Isotropic chemical shifts were calculated with an *RMSD* of 2.5 ppm (general conversion equation) or 1.6 ppm (conversion equation for magnesium phosphates). The quality of the results is similar to those reported for calcium phosphates obtained by GIPAW calculations[16].

In contrast to NMR calculations with periodic boundary conditions the EEIM makes use of the locality of NMR properties. An obvious advantage is the applicability to large unit cells. Also, defect structures can be examined efficiently. The EEIM can be readily used to calculate electric field gradients (EFGs) and J-couplings. It may be combined with true *ab initio* quantum chemical models that treat electron correlation on a more sophisticated level than the currently available density functionals. QM:QM embedding models for the QC region may help to make such calculations affordable. Desirable improvements of the EEIM are a fully automated QC setup and further refinement of the QC boundary treatment.

8 Acknowledgements

We like to thank Yamini Avadhut, Christian Minke, Marius Schulte and Melarie Davies for assistance in the experimental characterization and synthesis of the phosphates and Prof. Dr. W. Schnick for providing the facilities at the chair of inorganic solid-state chemistry. This work was funded by the Deutsche Forschungsgemeinschaft (DFG, Emmy-Noether program SCHM1570-2/1).

References

[1] D. Stueber, *Concepts Magn. Reson.*, 2006, **28A**, 347–366.

[2] J. Schmedt auf der Günne, *J. Magn. Reson.*, 2003, **165**, 18–32.

[3] S. Un and M. P. Klein, *J. Am. Chem. Soc.*, 1989, **111**, 5119–5124.

[4] R. Tycko, D. P. Weliky and A. E. Berger, *J. Chem. Phys.*, 1996, **105**, 7915–7930.

[5] (*a*) R. K. Harris, S. Cadars, L. Emsley, J. R. Yates, C. J. Pickard, R. K. R. Jetti and U. J. Griesser, *Phys. Chem. Chem. Phys.*, 2007, **9**, 360–368; (*b*) D. N. Brouwer, *J. Magn. Reson.*, 2008, **194**, 136–146.

[6] K. J. D. MacKenzie and M. E. Smith, *Multinuclear Solid-State NMR of Inorganic Materials*, Pergamon, London, 2002, vol. 6.

[7] (*a*) L. M. Bull, B. Bussemer, T. Anupõld, A. Reinhold, A. Samoson, J. Sauer, A. K. Cheetham and R. Dupree, *J. Am. Chem. Soc.*, 2000, **122**, 4948–4958; (*b*) S. Berger, S. Braun and H.-O. Kalinowski, ^{31}*P-NMR-Spektroskopie*, Georg Thieme Verlag, Stuttgart (Germany), 1993, vol. 3; (*c*) S. Berger, S. Braun and H.-O. Kalinowski, ^{19}*F-NMR-Spektroskopie*, Georg Thieme Verlag, Stuttgart (Germany), 1994, vol. 4.

[8] J. S. Knyrim, F. M. Schappacher, R. Pöttgen, J. Schmedt auf der Günne, D. Johrendt and H. Huppertz, *Chem. Mater.*, 2007, **19**, 254–262.

[9] (*a*) J. Gauss and J. F. Stanton, *Adv. Chem. Phys.*, 2002, **123**, 355–422; (*b*) A. A. Auer, J. Gauss and J. F. Stanton, *J. Chem. Phys.*, 2003, **118**, 10407–10417.

[10] C. J. Pickard and F. Mauri, *Phys. Rev. B*, 2001, **63**, 245101.

[11] M. Parrinello, J. Hutter, D. Marx, P. Focher, M. Tuckerman, W. Andreoni, A. Curioni, E. Fois, U. Roetlisberger, P. Giannozzi, T. Deutsch, A. Alavi, D. Sebastiani, A. Laio, J. Van de Vondele, A. Seitsonen and S. B. *et al.*, *CPMD 3.11*, MPI für Festkörperforschung Stuttgart 1997-2001, IBM Corp. 1990-2006 technical report, 2006.

[12] (*a*) D. Sebastiani and M. Parinello, *J. Phys. Chem.*, 2001, **A 105**, 1951–1958; (*b*) D. Sebastiani, G. Goward, I. Schnell and M. Parinello, *Comp. Phys. Comm.*, 2002, **147**, 707–710.

[13] S. J. Clark, M. D. Segall, C. J. Pickard, P. J. Hasnip, M. J. Probert, K. Refson and M. C. Payne, *Z. Kristallogr.*, 2005, **220**, 567–570.

[14] D. Raczkowski, A. Canning, L. Wang, S. G. Louie, B. Pfrommer, Y. Yoon, M. L. Cohen, D. R. amd F. Mauri, M. Cote, C. Pickard, P. Haynes and J. Yates, *PARATEC (PARAllel Total Energy Code).*, http://www.nersc.gov/projects/paratec/, 2007.

[15] F. Mauri, B. Pfrommer and S. Louie, *Phys. Rev. Lett.*, 1996, **77**, 5300–5303.

[16] F. Pourpoint, A. Kolassiba, C. Gervais, T. Azaïs, L. Bonhomme-Coury, C. Bonhomme and F. Mauri, *Chem. Mater.*, 2007, **19**, 6367–6369.

[17] W. Kutzelnigg, U. Fleischer and M. Schindler, *The IGLO-Method: Ab-initio Calculation and Interpretation of NMR Chemical Shifts and Magnetic Susceptibilities*, in *NMR – Basic Principles and Progress*, ed. P. Diehl, E. Fluck, H. Günther, R. Kosfeld and J. Seelig, Springer, 1991, vol. 23, pp. 165–262.

[18] G. Schreckenbach and T. Ziegler, *Int. J. Quantum Chem.*, 1996, **60**, 753–766.

[19] D. Stueber, F. N. Gunneau and D. M. Grant, *J. Chem. Phys.*, 2001, **114**, 9236–9243.

[20] M. Strohmeier, D. Stueber and D. M. Grant, *J. Phys. Chem.*, 2003, **A107**, 7629–7642.

[21] D. Stueber and D. M. Grant, *J. Am. Chem. Soc.*, 2002, **124**, 10539–10551.

[22] H. Lin and D. G. Truhlar, *Theor. Chem. Acc.*, 2007, **117**, 185–199.

[23] A. M. Orendt, *Magn. Reson. Chem.*, 2006, **44**, 385–389.

[24] Y. Zhang and E. Oldfield, *J. Phys. Chem.*, 2004, **B108**, 19533–19540.

[25] M.-S. Liao and Q.-E. Zhang, *J. Solid State Chem.*, 1999, **146**, 239–244.

[26] T. Bredow, *Int. J. Quantum Chem.*, 1999, **75**, 127–132.

[27] P. Reinhard, M. Causà, C. Marian and B. A. Hess, *Phys. Rev. B*, 1996, **54**, 14812–14821.

[28] J. A. Mejías and J. F. Sanz, *J. Chem. Phys.*, 1995, **102**, 327–336.

[29] C. Sousa, J. Casanovas, J. Rubio and F. Illas, *J. Comp. Chem.*, 1993, **14**, 680–684.

[30] A. DeDios, J. G. Pearson and E. Oldfield, *Science*, 1993, **260**, 1491–1496.

[31] (*a*) N. W. Winter, R. M. Pitzer and D. K. Temple, *J. Chem. Phys.*, 1987, **86**, 3549–3556; (*b*) N. W. Winter, R. M. Pitzer and D. K. Temple, *J. Chem. Phys.*, 1987, **87**, 2945–2953.

[32] A. M. Köster, P. Calaminici, M. E. Casida, R. Flores-Moreno, G. Geudtner, A. Goursot, T. Heine, A. Ipatov, F. Janetzko, J. M. del Campo, S. Patchkovskii, J. U. Reveles, D. R. Salahub and d. d. A Vela, *deMon2k*, http://www.demon-software.com, 2006.

[33] *DALTON, a molecular electronic structure program, Release 2.0 (2005)*, full reference given in supplemental material.

[34] J. F. Stanton and J. Gauss *et al.*, *Aces II, Mainz-Austin-Budapest version (2008)*, http://www.aces2.de, full reference given in the supplemental material.

[35] J. F. Stanton, J. Gauss, J. D. Watts, W. J. Lauderdale and R. J. Bartlett, *Int. J. Quantum Chem. Symp.*, 1992, **26**, 879–894.

[36] L. Visscher, H. J. A. Jensen and T. S. with new contributions from R. Bast, S. Dubillard, K. G. Dyall, U. Ekström, E. Eliav, T. Fleig, A. S. P. Gomes, T. U. Helgaker, J. Henriksson, M. Ilias, Ch. R. Jacob, S. Knecht, P. Norman, J. Olsen, M. Pernpointner, K. Ruud, P. Salek, and J. Sikkema, *Dirac, a relativistic ab initio electronic structure program, Release DIRAC08 (2008)*, http://dirac.chem.sdu.dk, 2008.

[37] M. S. Gordon and M. W. Schmidt, *Advances in electronic structure theory: GAMESS a decade later*, in *Theory and Applications of Computational Chemistry: the first forty years*, ed. C. E. Dykstra, G. Frenking, K. S. Kim and G. E. Scuseria, Elsevier, Amsterdam, 2005, ch. 41, pp. 1167–1189.

[38] F. Neese, *ORCA – an ab initio, Density Functional and Semiempirical program package, Version 2.6*, University of Bonn, Bonn (Germany), 2008.

[39] C. van Wüllen and W. Kutzelnigg, *Chem. Phys. Lett.*, 1993, **205**, 563–571.

[40] J. Autschenbach, *Calculation of Heavy-Nucleus Chemical Shifts. Relativistic All-Electron Methods*, in *Calculation of NMR and EPR Parameters - Theory and Applications*, ed. M. Kaupp, M. Bühl and V. G. Malkin, Wiley-VCH, 2004, ch. 14, pp. 227–247.

[41] M. J. Frisch *et al.*, *Gaussian 03, Revision D.01*, 2004, full reference given in supplemental material.

[42] E. J. Baerends *et al.*, *ADF – Amsterdam Density Functional software, ver. 2007.01*, http://www.scm.com, full reference given in supplemental material.

[43] S. A. Joyce, J. R. Yates, C. J. Pickard and F. Mauri, *J. Chem. Phys.*, 2007, **127**, 204107.

[44] N. F. Ramsey, *Phys. Rev.*, 1950, **78**, 699–703.

[45] A. Saika and C. P. Slichter, *J. Chem. Phys.*, 1954, **22**, 26–28.

[46] H. M. McConnell, *J. Chem. Phys.*, 1957, **27**, 226–229.

[47] J. A. Pople, *J. Chem. Phys.*, 1962, **37**, 53–59.

[48] J. Mason, *J. Chem. Soc., Faraday Trans. 2*, 1977, **73**, 1464–1474.

[49] C. J. Jameson and A. C. de Dios, *J. Chem. Phys.*, 1992, **97**, 417–434.

[50] C. J. Jameson and A. C. de Dios, *J. Chem. Phys.*, 1993, **98**, 2208–2217.

[51] A. Barszczewicz, M. Jaszunski, T. Helgaker and K. Ruud, *Chem. Phys. Lett.*, 1996, **250**, 1–8.

[52] R. A. Hegstrom, *Phys Rev.*, 1979, **A19**, 17–30.

[53] D. Stueber and D. M. Grant, *Solid State NMR*, 2002, **22**, 439–457.

[54] E. V. Stefanovich and T. N. Truong, *J. Phys. Chem.*, 1998, **B102**, 3018–3022.

[55] M. Klintenberg, S. E. Derenzo and M. J. Weber, *Comp. Phys. Commun.*, 2000, **131**, 120–128.

[56] S. E. Derenzo, M. K. Klintenberg and M. J. Weber, *J. Chem. Phys.*, 2000, **112**, 2074–2081.

[57] J. Almlöf and U. Wahlgren, *Theor. Chim. Acta*, 1973, **28**, 161–168.

[58] P. P. Ewald, *Ann. Phys.*, 1921, **369**, 253–287.

[59] B. G. Johnson, P. M. W. Gill, J. A. Pople and D. J. Fox, *Chem. Phys. Lett.*, 1993, **206**, 239–246.

[60] M.-S. Liao and Q.-E. Zhang, *Inorg. Chem.*, 1997, **36**, 396–405.

[61] H. M. Evjen, *Phys. Rev.*, 1932, **39**, 675–687.

[62] S. Y. Shashkin and W. A. Goddard III, *Phys. Rev. B*, 1986, **33**, 1353–1359.

[63] N. E. Brener and J. Callaway, *Phys. Rev. B*, 1987, **35**, 4001–4009.

[64] Q. Cui and M. Karplus, *J. Chem. Phys.*, 2000, **B 104**, 3721–3743.

[65] R. S. Mulliken, *J. Chem. Phys.*, 1955, **23**, 1833–1840.

[66] A. Reed, R. B. Weinstock and F. Weinhold, *J. Chem. Phys.*, 1985, **83**, 735–746.

[67] E. R. Davidson, *J. Chem. Phys.*, 1967, **46**, 3320–3324.

[68] K. R. Roby, *Mol. Phys.*, 1974, **27**, 81–104.

[69] R. Heinzmann and R. Ahlrichs, *Theor. Chim. Acta*, 1976, **42**, 33–45.

[70] F. A. Momany, *J. Phys. Chem.*, 1978, **82**, 592–601.

[71] S. R. Cox and D. E. Williams, *J. Comp. Chem.*, 1981, **2**, 304–323.

[72] U. C. Singh and P. A. Kollman, *J. Comp. Chem.*, 1984, **5**, 129–145.

[73] L. Chirlian and M. Francl, *J. Comp. Chem.*, 1987, **8**, 894–905.

[74] C. M. Breneman and K. B. Wiberg, *J. Comp. Chem.*, 1990, **11**, 361–373.

[75] M. M. Francl, C. Carey, L. E. Chirlian and D. M. Gange, *J. Comp. Chem.*, 1996, **17**, 367–383.

[76] R. W. F. Bader, *Atoms In Molecules, A Quantum Theory*, Clarendon, Oxford, 1990.

[77] I. V. Yudanov, V. A. Nasluzov, K. M. Neyman and N. Rösch, *Int. J. Quantum Chem.*, 1997, **65**, 975–986.

[78] G. G. Hall, *Theor. Chim. Acta*, 1983, **63**, 357–364.

[79] C. M. Smith and G. G. Hall, *Theor. Chim. Acta*, 1986, **69**, 63–70.

[80] J. Gao, *Methods and Applications of Combined Quantum Mechanical and Molecular Mechanical Potentials*, in *Reviews in Computational Chemistry*, ed. K. B. Lipkowitz and D. B. Boyd, VCH Publishers, 1996, vol. 7, ch. 3, pp. 119–185.

[81] R. D. J. Froese and K. Morokuma, *Hybrid Methods*, in *Encyclopedia of Computational Chemistry*, ed. P. v. R. Schleyer *et al.*, Wiley & Sons, New York, 1998, pp. 1244–1256.

[82] V. Théry, D. Rinaldi, J. Rivail, B. Maigret and G. G. Ferenczy, *J. Comp. Chem.*, 1994, **15**, 269–282.

[83] J. Gao, P. Amara, C. Alhambra and M. C. Field, *J. Phys. Chem.*, 1998, **A102**, 4714–4721.

[84] J. Gauss and H.-J. Werner, *Phys. Chem. Chem. Phys.*, 2000, **2**, 2083–2090.

[85] C. R. Jacob and L. Visscher, *J. Chem. Phys.*, 2006, **125**, 194104.

[86] (*a*) T. Jacob, D. Geschke, S. Fritzsche, W. Sepp, B. Fricke, J. Anton and S. Varga, *Surf. Sci.*, 2001, **486**, 194–202; (*b*) T. Jacob, *Ph.D. thesis*, University of Kassel, Germany, 2002.

[87] T. Helgaker, M. Jaszuński and K. Ruud, *Chem. Rev.*, 1999, **99**, 293–352.

[88] (*a*) K. Wolinski, J. F. Hinton and P. Pulay, *J. Am. Chem. Soc.*, 1990, **112**, 8251–8265; (*b*) F. London, *J. Phys. Radium*, 1937, **8**, 397–409; (*c*) H. F. Hameka, *Mol. Phys.*, 1958, **1**, 203–215; (*d*) R. Ditchfield, *Mol. Phys.*, 1974, **27**, 789–807.

[89] E. Anderson, Z. Bai, C. Bischof, S. Blackford, J. Demmel, J. Dongarra, J. Du Croz, A. Greenbaum, S. Hammarling, A. McKenney and D. Sorensen, *LAPACK Users' Guide*, Society for Industrial and Applied Mathematics, Philadelphia, PA, 3rd edn., 1999.

[90] *Intel Math Kernel Library, ver. 10.0.1.014*, Intel Corporation Technical Report Document Number: 314664-005US, 2006–2008.

[91] Advanced Micro Devices, Inc., Numerical Algorithms group, Ltd., http://developer.amd.com/cpu/libraries/acml, *AMD Core Math Library (ACML), ver. 4.1.0*, 2003–2008.

[92] D. Stueber, A. M. Orendt, J. C. Facelli, R. W. Parry and D. M. Grant, *Solid State Nucl. Magn. Reson.*, 2002, **22**, 29–49.

[93] U. Groß, S. Rüdiger, A. Grimmer and E. Kemnitz, *J. Fluor. Chem.*, 2002, **115**, 193–199.

[94] A. D. Buckingham and S. M. Malm, *Mol. Phys.*, 1971, **22**, 1127–1130.

[95] D. B. Chesnut, B. E. Rusiloski, K. D. Moore and D. A. Egolf, *J. Comp. Chem.*, 1993, **14**, 1364–1375.

[96] D. B. Chesnut and E. F. C. Byrd, *Chem. Phys.*, 1996, **213**, 153–158.

[97] W. T. Pennington, *J. Appl. Cryst.*, 1999, **32**, 1028–1029.

[98] L. Wall, T. Christiansen and J. Orwant, *Programming Perl*, O'Reilly Media, Sebastopol, CA 95472 (USA), 3rd edn., 2000.

[99] J. W. Jeffery, in *Methods in X-Ray Crystallography*, Academic Press, London, 1971, p. 333f.

[100] C. Adamo and V. Barone, *J. Chem. Phys.*, 1998, **108**, 664–675.

[101] E. D. Glendering, J. K. Badenhoop, A. E. Reed, J. E. Carpenter, J. A. Bohmann, C. M. Morales and F. Weinhold, *NBO 5.0*, Theoretical Chemistry Institute, University of Wisconsin, Madison, 2001.

[102] V. A. Streltsov, V. G. Tsirelson, R. P. Ozerov and O. A. Golovanov, *Kristallografiya*, 1988, **33**, 90–97.

[103] P. Hewat, *Inorganic Crystal Structure Database (ICSD-for-WWW)*, Fachinformationszentrum Karlsruhe (FIZ), Release 2006-2 edn.

[104] R. K. Harris, E. D. Becker, S. M. Cabral de Menezes, R. Goodfellow and P. Granger, *Solid State NMR*, 2002, **22**, 458–483.

[105] D. R. Lide, *CRC Handbook of Chemistry and Physics, CDROM Version*, CRC Press, 2003.

[106] D. K. Hindermann and C. D. Cornwell, *J. Chem. Phys.*, 1968, **48**, 4148–4154.

[107] A. Nord and K. B. Lindberg, *Acta. Chem. Scand.*, 1975, **A29**, 1–6.

[108] A. G. Nord and P. Kierkegaard, *Acta Chem. Scand.*, 1968, **22**, 1466–1474.

[109] C. Calvo, *Acta Cryst.*, 1967, **23**, 289–295.

[110] D. Stachel, H. Paulus, C. Guenter and H. Fuess, *Z. Kristallogr.*, 1992, **199**, 275–276.

[111] R. Krishnan, J. Binkley, R. Seeger and J. Pople, *J. Chem. Phys.*, 1980, **72**, 650–654.

[112] A. D. McLean and G. S. Chandler, *J. Chem. Phys.*, 1980, **72**, 5639–5648.

[113] J. Blaudeau, M. P. McGrath, L. A. Curtiss and L. Radom, *J. Chem. Phys.*, 1997, **107**, 5016–5021.

[114] P. C. Hariharan and J. A. Pople, *Theor. Chim. Acta*, 1973, **28**, 213–222.

[115] M. M. Francl, W. J. Petro, W. J. Hehre, J. S. Binkley, M. S. Gordon, D. J. DeFrees and J. A. Pople, *J. Chem. Phys.*, 1982, **77**, 3654–3665.

[116] V. Rassolov, J. A. Pople, M. Ratner and T. Windus, *J. Chem. Phys.*, 1998, 1223–1129.

[117] W. J. Stevens, H. Basch and M. Krauss, *J. Chem. Phys.*, 1984, **81**, 6026–6033.

[118] Stoe & Cie GmbH, Hilpertstr. 10, D-64295 Darmstadt, *Stoe WINPOW, ver.2.12*, 2005.

[119] M. Bak, J. T. Rasmussen and N. C. Nielsen, *J. Magn. Reson.*, 2000, **147**, 296–330.

[120] U. Haeberlen, *High Resolution NMR in Solids*, Academic Press, New York, 1976.

[121] A. F. Wells, *Structural inorganic chemistry*, Clarendon Press, Oxford, 4th edn., 1975.

[122] W. Vogel, *Glaschemie*, Springer, Berlin, 3rd edn., 1992.

[123] A. K. Cheetham, N. J. Clayden, C. M. Dobson and R. J. B. Jakeman, *J. Chem. Soc., Chem. Commun.*, 1986, 195–197.

[124] F. Fayon, D. Massiot, K. Suzuya and D. L. Price, *J. Non-Cryst. Solids*, 2001, **283**, 88–94.

[125] M. Feike, D. E. Demco, R. Graf, J. Gottwald, S. Hafner and H. W. Spiess, *J. Magn. Reson.*, 1996, **A122**, 214–221.

[126] M. A. Aramendía, V. Borau, C. Jiménez, J. M. Marinas, F. J. Romero and J. R. Ruiz, *J. Colloid Interface Sci.*, 1998, **202**, 456–461.

[127] K. Łukaszewicz, *Bull. Acad. Pol. Sci. Chim.*, 1967, **15**, 53–57.

[128] M. Feike, R. Graf, I. Schnell, C. Jäger and H. W. Spiess, *J. Am. Chem. Soc.*, 1996, **118**, 9631–9634.

[129] B. Moreno, C. O. Rodriguez, B. N. Bailey, J. A. Urbina, S. N. J. Moreno, R. Docampo and E. Oldfield, *FEBS Lett.*, 2002, **523**, 207–212.

[130] K. O. Kongshaug, H. Fjellvag and K. P. Lillerud, *Solid State Sci.*, 2000, **2**, 205–214.

[131] C. Calvo, *Can. J. Chem.*, 1965, **43**, 1139–1146.

[132] K. Łukaszewicz, *Roczniki Chemii*, 1961, **35**, 31–35.

[133] D. N. Brouwer and G. D. Enright, *J. Am. Chem. Soc.*, 2008, **130**, 3095–3105.